Received: 6 December 2019 | Accepted: 16 April 2020

DOI: 10.1111/gcb.15138

PRIMARY RESEARCH ARTICLE

Global Change Biology WILEY

Nutrients and water availability constrain the seasonality of vegetation activity in a Mediterranean ecosystem

Yunpeng Luo[1] | Tarek El-Madany[1] | Xuanlong Ma[1,2] | Richard Nair[1] | Martin Jung[1] | Ulrich Weber[1] | Gianluca Filippa[3] | Solveig F. Bucher[4,5] | Gerardo Moreno[6] | Edoardo Cremonese[3] | Arnaud Carrara[7] | Rosario Gonzalez-Cascon[8] | Yonatan Cáceres Escudero[9] | Marta Galvagno[3] | Javier Pacheco-Labrador[1] | M. Pilar Martín[10] | Oscar Perez-Priego[11] | Markus Reichstein[1,5] | Andrew D. Richardson[12,13] | Annette Menzel[14] | Christine Römermann[2,4,5] | Mirco Migliavacca[1]

[1]Department for Biogeochemical Integration, Max-Planck-Institute for Biogeochemistry, Jena, Germany

[2]German Centre for Integrative Biodiversity Research (iDiv) Halle-Jena-Leipzig, Leipzig, Germany

[3]Environmental Protection Agency of Aosta Valley, ARPA Valle d'Aosta, Aosta, Italy

[4]Plant Biodiversity Group, Institute of Ecology and Evolution, Friedrich Schiller University Jena, Jena, Germany

[5]Michael-Stifel-Center Jena for Data-Driven and Simulation Science, Jena, Germany

[6]Institute for Dehesa Research, University of Extremadura, Plasencia, Spain

[7]Fundación Centro de Estudios Ambientales del Mediterráneo (CEAM), Paterna, Spain

[8]Department of Environment, National Institute for Agriculture and Food Research and Technology (INIA), Madrid, Spain

[9]Forestry School, University of Extremadura, Plasencia, Spain

[10]Environmental Remote Sensing and Spectroscopy Laboratory (SpecLab), Institute of Economic, Geography and Demography (IEGD-CCHS), Spanish National Research Council (CSIC), Madrid, Spain

[11]Department of Biological Sciences, Macquarie University, North Ryde, NSW, Australia

[12]School of Informatics, Computing and Cyber Systems, Northern Arizona University, Flagstaff, AZ, USA

[13]Center for Ecosystem Science and Society, Northern Arizona University, Flagstaff, AZ, USA

[14]Department of Ecology and Ecosystem Management, TUM School of Life Sciences, Technical University of Munich, Freising, Germany

Correspondence
Yunpeng Luo and Mirco Migliavacca, Department for Biogeochemical Integration, Max-Planck-Institute for Biogeochemistry, 07745 Jena, Germany.
Email: yluo@bgc-jena.mpg.de (Y. L.); mmiglia@bgc-jena.mpg.de (M. M.)

Funding information
Regional Government of Extremadura, Grant/Award Number: IB16185; Alexander von Humboldt Foundation

Abstract

Anthropogenic nitrogen (N) deposition and resulting differences in ecosystem N and phosphorus (P) ratios are expected to impact photosynthetic capacity, that is, maximum gross primary productivity (GPP_{max}). However, the interplay between N and P availability with other critical resources on seasonal dynamics of ecosystem productivity remains largely unknown. In a Mediterranean tree–grass ecosystem, we established three landscape-level (24 ha) nutrient addition treatments: N addition (NT), N and P addition (NPT), and a control site (CT). We analyzed the response of ecosystem to altered nutrient stoichiometry using eddy covariance fluxes measurements, satellite observations, and digital repeat photography. A set of metrics, including phenological transition dates (PTDs; timing of green-up and dry-down), slopes during green-up and

[Correction added on 09 June 2020, after first online publication: the copyright line and legal statement have been updated in this current version.]

dry-down period, and seasonal amplitude, were extracted from time series of GPP_{max} and used to represent the seasonality of vegetation activity. The seasonal amplitude of GPP_{max} was higher for NT and NPT than CT, which was attributed to changes in structure and physiology induced by fertilization. PTDs were mainly driven by rainfall and exhibited no significant differences among treatments during the green-up period. Yet, both fertilized sites senesced earlier during the dry-down period (17–19 days), which was more pronounced in the NT due to larger evapotranspiration and water usage. Fertilization also resulted in a faster increase in GPP_{max} during the green-up period and a sharper decline in GPP_{max} during the dry-down period, with less prominent decline response in NPT. Overall, we demonstrated seasonality of vegetation activity was altered after fertilization and the importance of nutrient–water interaction in such water-limited ecosystems. With the projected warming-drying trend, the positive effects of N fertilization induced by N deposition on GPP_{max} may be counteracted by an earlier and faster dry-down in particular in areas where the N:P ratio increases, with potential impact on the carbon cycle of water-limited ecosystems.

KEYWORDS

GPP capacity, nitrogen deposition, nutrient imbalance, phenology, random forest, semi-arid, structure and physiology, tree–grass ecosystem, water availability

1 | INTRODUCTION

Gross primary productivity (GPP), the most important component of the terrestrial carbon cycle (Beer et al., 2010; Ciais et al., 2014), varies greatly over space and time. A better understanding of its temporal variability is crucial to accurately predict carbon fluxes under global changes (Xia et al., 2015). At the seasonal time scale, variability of GPP is controlled mainly by the dynamics of vegetation structure (Richardson et al., 2013), such as leaf area index (LAI), which is monitored using vegetation indexes (VIs) from remote (Zhang et al., 2003) or near-surface sensing measurements (Richardson, Braswell, Hollinger, Jenkins, & Ollinger, 2009). Therein, land-surface phenology (the timing of recurrent biological events such as the start of the green-up or dry-down of canopy), slopes and amplitudes of the seasonal cycle are often extracted from time series of VIs (Gerard, George, Hayman, Chavana-Bryant, & Weedon, 2020; Liu et al., 2016) used as metrics to describe the seasonal dynamics of canopy structural development (Soudani et al., 2012). Similarly, maximum gross primary productivity (GPP_{max}), representing the carbon sequestration potential of vegetation activity (i.e., photosynthetic capacity) and dominating the interannual variability of global net ecosystem exchange (NEE; Fu et al., 2019), in conjunction with extracted metrics from its time series, can also be used to describe seasonal variation of GPP.

Attention has been paid to canopy development and its phenology in terms of its response to both long-term climate (Cleland, Chuine, Menzel, Mooney, & Schwartz, 2007; Menzel et al., 2006; Wang et al., 2015) and short-term weather (de Jong, Verbesselt, Schaepman, & de Bruin, 2012). Likewise, seasonality of vegetation activity is also strongly affected by climate and meteorological factors (Richardson et al., 2010; Wingate et al., 2015). However, plants simultaneously balance uptake of multiple resources (i.e., carbon, nutrients, and water), and alter allocation to maximize acquisition of the most limiting resource (Bloom, Chapin, & Mooney, 1985; Chapin, Schulze, & Mooney, 1990). This means that both background ecosystem nutrient stoichiometry (e.g., N:P ratio) and the threefold increase in anthropogenic nitrogen deposition (Peñuelas, Sardans, Rivas-ubach, & Janssens, 2012; Reay, Dentener, Smith, Grace, & Feely, 2008) may alter seasonality of vegetation activity and phenology due to variations in nutrient availability (Piao et al., 2019). In particular, as anthropogenic N deposition (Reay et al., 2008) is far in excess of P deposition and mineral weathering (Mahowald et al., 2008; Peñuelas et al., 2012), the observed general shift toward a higher N:P ratio is expected to exert impacts on macro-scale ecosystem functioning and properties (Fay et al., 2015; Janssens et al., 2010). Previous studies show that changing N or P availability can change the timing of leaf unfolding and extension (Yang, Zavišić, Pena, & Polle, 2016) as well as the growing season length (Wang & Tang, 2019). Plants under different soil nutrients stoichiometry differ in uptake and transport of nutrients (Yang et al., 2016), which would further affect canopy structural development (Jing et al., 2017) and photosynthetic rate (Yang et al., 2016). As a result, changes in N:P ratio can alter the periodicity and magnitude of seasonal changes in both structural and functional properties of ecosystems (i.e., canopy structure and photosynthetic capacity). Understanding the links between nutrient availability and seasonal patterns of photosynthetic capacity (e.g., phenology of GPP_{max}) is thus crucial to understand temporal

patterns in biosphere–atmosphere carbon exchange (Migliavacca et al., 2015; Piao et al., 2019).

Few previous studies have considered nutrient effects on phenology and seasonality of vegetation activity, mostly focusing on leaf-level or individual plants at plot scale (Burner, Brauer, Snider, Harrington, & Moore, 2014; Peñuelas et al., 2013; Serrano, Filella, & Peñuelas, 2000). Those studies are valuable to explore the response of plants to different nutrient availability. However, due to limited sampling frequency, they normally cannot be used to quantify changes in canopy development and vegetation activity at high temporal resolution (e.g., daily). More importantly, they are limited in considering the integrated ecosystem response. For instance, they are limited to quantify the effects of interactions between the ecosystem compartments, for example, the interspecific competition among plants and feedbacks between plants, soil, and meteorology.

Few studies on nutrient and water interaction have been conducted in the semi-arid tree–grass ecosystem (Nomura & Kikuzawa, 2003; Xia & Wan, 2013; Yin, Zheng, Cao, Song, & Yu, 2016). One particularly understudied system is located in Mediterranean climate zones, where typical tree–grass systems have complex structure and changing limiting resources throughout the year, with water limitations in the summer dry season, nutrient limitations in the rainy seasons (Moreno, 2008; Morris, Nair, Moreno, Schrumpf, & Migliavacca, 2019; Nair et al., 2019; Sardans & Peñuelas, 2013). These complex interactions imply that determining the interlinkage between nutrients (i.e., N and P) and water availability in shaping vegetation phenology and its activity in such ecosystems is a major challenge (Piao et al., 2019). Besides, water variability in such seasonally dry systems is important (Forkel et al., 2015; Jung et al., 2017; Zeng, Mariotti, & Wetzel, 2005) as it is the main environmental driver of carbon fluxes, which dominate the interannual variability of global carbon fluxes (Ahlström et al., 2015; Poulter et al., 2014).

In addition, the variability of vegetation activity can be attributed to changes in vegetation structure (e.g., LAI or biomass) and physiological factors (e.g., light use efficiency [LUE]; Hu et al., 2018; Richardson, Hollinger, Aber, Ollinger, & Braswell, 2007; Wu et al., 2012). Decoupling the contribution of structure and physiology to vegetation activity at high resoultion (i.e., daily) is helpful to elucidate the effect of nutrient availability on the seasonal dynamics of these ecosystems.

In this study, we used data from a large-scale (24 ha) nutrient (N and P) manipulation experiment (MANIP: https://www.bgc-jena.mpg.de/bgi/index.php/Research/Manip) conducted in a Mediterranean tree–grass ecosystem characterized by a high seasonal dynamic. The experiment was designed to provide an excess of N (mimicking the effects of 10 years of atmospheric N deposition), resulting in imbalanced N:P ratios in the footprint of one eddy covariance (EC) tower (NT) and relieve the imbalance by adding N and P together at the footprint of another tower (NPT). In addition, one tower site was kept as control (CT) without any nutrient addition (El-Madany et al., 2018). A P only treatment was not included because a trial fertilization on the herbaceous layer and the N:P ratio of vegetation show that the ecosystem is rather N-limited than P-limited and it does not respond to P fertilization alone (Migliavacca et al., 2017; Nair et al., 2019). We jointly used eddy flux observation, satellite data, and digital repeat photography (El-Madany et al., 2018; Luo et al., 2018) to define metrics of the seasonality, namely phenological transition dates (PTDs), the start of critical phenological events such as the start of green-up or dry-down; amplitudes of the seasonal cycle and slopes in the green-up and dry-down periods as rates of change (Luo et al., 2018). With these high-resolution data and extracted metrics, combining with other measured environmental factors, we aim to answer the following questions (Figure 1):

1. How do nutrient availability and stoichiometry influence the seasonality of canopy development and photosynthetic capacity (GPP_{max})?
2. How do water availability and its interaction with nutrients drive the observed differences in GPP_{max}?
3. Are the observed changes in GPP_{max} after fertilization due to changes in vegetation structure or due to physiological changes?

A schematic representation of the three questions addressed in this study is reported in Figure 1. Considering the characteristics of the Mediterranean climate (rainy autumn–winter, and warm and dry summer) and shape of the time series of canopy structure and photosynthetic capacity (two peaks in late autumn and spring, respectively), we adopted the concept of "hydrological years" as described in Luo et al. (2018)—a year defined from 1 September to 31 August. In this study, we mainly focus on the green-up at the autumn–winter period (green-up), the peak of GPP_{max} (spring peak), and dry-down in the late spring–summer period (dry-down) as those periods are most important and sensitive to detect the ecosystem response to environmental changes (Luo et al., 2018).

2 | MATERIALS AND METHODS

2.1 | Description of experimental sites and instruments set-up

The three experimental sites are located in Majadas de Tiétar, Cáceres, Spain (39°56′24.68″N, 5°46′28.70″W). It is a Mediterranean tree–grass ecosystem, composed of a dominant herbaceous layer and low density (~20%; El-Madany et al., 2018) evergreen broadleaf oak trees (*Quercus ilex* L.). The annual mean air temperature of Majadas de Tiétar is 16.7°C. The annual precipitation approximates 650 mm and falls typically from November to May with a very dry summer (Luo et al., 2018; Perez-Priego et al., 2017). An initial dose of phosphorus fertilizer (50 kg P/ha as triple superphosphate, $Ca(H_2PO_4)_2$) was applied at NPT in

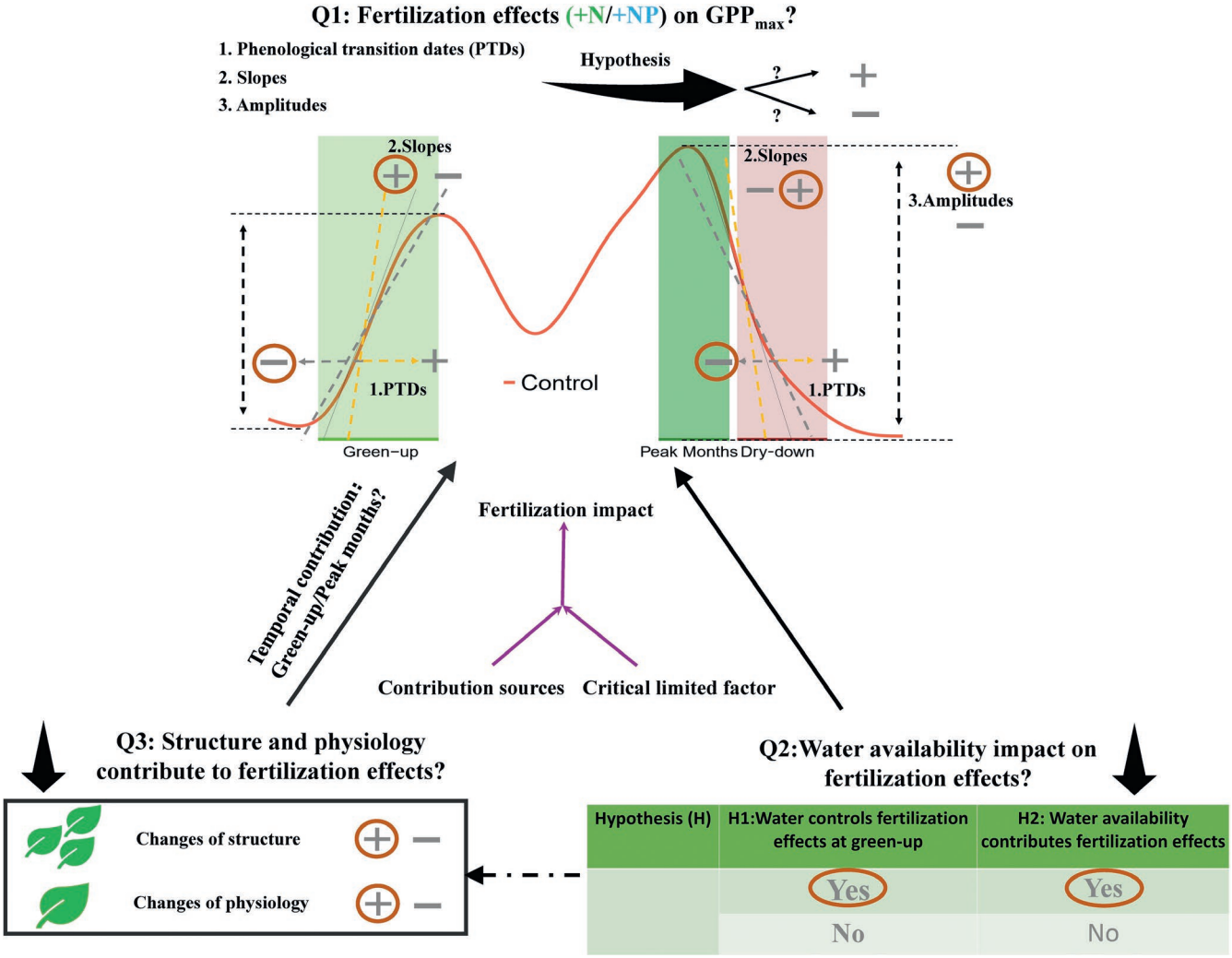

FIGURE 1 Illustration of research questions in this study. (1) How do nutrient availability and stoichiometry influence the daily maximum gross primary productivity (GPP_{max})? (2) How do the crucial environmental factors, specifically water availability, interact with the nutrient availability? (3) Are changes in structure and changes in physiology contributing to the variation in GPP_{max} and at which periods are they contributing? In this schematic plot, the "+" stands for the increase in properties or positive contribution, while "–" represents the decrease in properties or negative contribution. "Yes" means supporting the hypotheses, while "No" represents that against the hypotheses. The brown circles are our original hypotheses

November 2014, followed by 100 kg N/ha at NT (in the form of calcium ammonium nitrate: $Ca(NO_3)_2NH_4NO_3$) and NPT (as ammonium nitrate: NH_3NO_3) in March 2015. At the end of February and early March 2016, a second dose of the same fertilizers was successively added into NT (20 kg N/ha) and NPT (10 kg P/ha and 20 kg N/ha), respectively. The total doses of N were approximately 10 times higher than the current N deposition rate in this area (Morris et al., 2019). The P addition in the NP site was calibrated to compensate for the N imbalance and maintain the original N:P stoichiometry of the ecosystem's herbaceous layer (Nair et al., 2019). The fertilization scheme was defined on the basis of a fully factorial small-scale fertilization experiment on the herbaceous layer (Migliavacca et al., 2017; Perez-Priego et al., 2015), which showed an N limitation at the experimental site and negligible response to P alone. This was also confirmed by the vegetation N:P stoichiometry at the site (both herbaceous layer and trees) that indicated an N limitation before fertilization (data not shown here). Moreover, it was logistically difficult to include a fourth treatment without overlap of the EC footprint climatology, given the large-scale fertilization applied (24 ha). For these reasons, we did not include in the experimental design a plot fertilized only with P.

An EC system was installed at 15 m height to measure the carbon, water, and energy fluxes at each site. Each EC system consisted of a three-dimensional sonic anemometer (R3-50; Gill LTD) and an infrared gas analyzer (LI-7200; LI-COR Bioscience) to measure mixing ratios of CO_2 and H_2O. Additional vertical CO_2 and H_2O concentration profiles were measured at seven levels (0.1, 0.5, 1.0, 2.0, 5.0, 9.0, and 15 m above ground with an LI-840; LI-COR Biosciences). Meteorological variables such as air temperature (T_a), shortwave incoming radiation (SW_{Rad}), incoming photosynthetically active radiation (PAR), vapor pressure deficit (VPD), and precipitation (Prec) were also measured at each site. Soil water

content (SWC) was measured at 0.05, 0.1, and 0.2 m below ground (ML2x; Delta-T Devices Ltd) with four replicated sensors in each site. The flux data were available from September 2013 in CT, and from March 2014 for NT and NPT. The SWC data were available from the end of November 2014 for all three sites (Figure S1 in the Supporting Information).

A digital camera (hereafter PhenoCam; Stardot NetCam, StarDot Technologies) facing north was mounted at the top of each EC tower. Images were taken every half hour (from 10:00 to 14:30 UTC) as JPEG format (Luo et al., 2018). The sequential Red, Blue, Green (RGB) images were collected by the PhenoCam. The field of views (FOVs) of cameras at NT and NPT were stable during the study period (from September 1, 2014 to August 31, 2018), whereas the FOV of CT was not constant and the camera had a white balance issue so the pictures cannot be compared over time until December 3, 2015. Hence, RGB images were available for the analysis from September 1, 2014 to August 31, 2018 for NT and NPT and from December 3, 2015 to August 31, 2018 for the CT site (Figure S1). Satellite images from the Landsat 8 Operational Land Imager (OLI) sensor from September 2013 to August 2018 were also selected to track the greenness changes in the experimental sites.

We summarized the main variables used in this study that were calculated from the above instruments and their roles in this study to better introduce the workflow in following method parts (Table 1).

Note ecosystem fluxes and properties before fertilization were compared between the three sites (El-Madany et al., 2018; Nair et al., 2019). Specifically, pre-treatment measurements both of soil (i.e., soil texture, soil C, N, and P) and leaf N and P of the herbaceous layer indicated no statistically significant difference among treatments (Nair et al., 2019). Additionally, El-Madany et al. (2018) evaluated the differences in carbon, energy, and water fluxes among NT, NPT, and CT before applying fertilization and demonstrated that they were not significantly different.

2.2 | Data for the characterization of photosynthetic capacity and canopy structure

2.2.1 | EC data processing and flux partitioning to GPP

EC data were collected at 20 Hz and then processed using EddyPro 6.2. The calculated CO_2 fluxes were then quality checked (Mauder & Foken, 2011; Rebmann et al., 2005) and corrected by adding storage fluxes (integrated CO_2 fluxes using seven levels of CO_2 profiles) to compute NEE. The friction velocity (u^*) thresholds were detected for each year and tower and u^* filtering was conducted following Papale et al. (2006).

The time series of NEE were gap filled using the marginal distribution sampling method (Reichstein et al., 2005). The portioning of NEE into GPP was conducted using nighttime-based methods (Reichstein et al., 2005). The calculation of fluxes was made according to El-Madany et al. (2018) and using the R package REddyProc v1.1.6 (Wutzler et al., 2018).

TABLE 1 Important variables used and their roles in this study

Data sourced	Variables	Research question	Roles
Processed	GPP_{max} (daily maximum gross primary productivity)	1, 2, 3	Representing photosynthetic capacity, used to extract PTDs, slopes, and amplitudes
	PhenoCam GCC (green chromatic coordinate)	1, 2	Representing canopy structure and used to extract PTDs
	Landsat NDVI (normalized difference vegetation index)	1, 3	Representing canopy structure and used to extract its slopes and amplitudes
	CSWI (conservative surface wetness index)	2	Used to compare ecosystem-scale water availability among treatments (evapotranspiration used in the calculation)
	WAI (soil water availability index)	2, 3	Used to represent water availability without using measured fluxes in the calculation; used in the random forest analysis
Measured	T_a (air temperature)	3	Meteorological drivers to predict GPP_{max} in random forest analysis
	VPD (vapor pressure deficit)		
	DL (day length)		
	Prec (Precipitation)	2	Used to characterize the rainfall
	SWC (soil water content)		Representing soil water content

Note: The numbers 1, 2, 3 indicate that the variables were used for the analysis targeting for the scientific questions 1, 2, 3, respectively (shown in Section 1).

Abbreviation: PTD, phenological transition date.

2.2.2 | Calculation of VIs from PhenoCam and Landsat 8

Digital numbers (DNs) of Red (R_{DN}), Green (G_{DN}), and Blue (B_{DN}) were extracted from each PhenoCam image and averaged over different regions of interest (ROIs, Figure S2). The green chromatic coordinate (GCC) was computed as in Equation (1; Richardson et al., 2007):

$$GCC = \frac{G_{DN}}{R_{DN} + G_{DN} + B_{DN}}. \quad (1)$$

Green chromatic coordinate was calculated individually from ROIs of trees and grasses and also at ecosystem scale considering grass and tree relative fractions within the tower footprint weighted by 0.8 and 0.2, respectively (Luo et al., 2018).

Atmospherically corrected surface reflectance products from Landsat 8-OLI (30 m spatial resolution and 16-day temporal resolution; https://www.usgs.gov/land-resources/nli/landsat/) from September 2013 to August 2018 were acquired. We used 450 m × 180 m rectangle (15 pixels × 6 pixels) around each EC tower according to the footprint climatology (El-Madany et al., 2018) to cut out the Landsat images. Then pixels with high data quality (i.e., pixels not contaminated by cloud or cirrus, shadow, and saturation) in the selected area of the images were chosen and near-infrared (NIR) and Red (R) reflectance bands were used to calculate normalized difference vegetation index (NDVI; Equation 2) according to Tucker (1979).

$$NDVI = \frac{NIR - R}{NIR + R}. \quad (2)$$

Normalized difference vegetation index was further averaged over each selected area to calculate the 16-day NDVI time series in each EC site.

2.2.3 | Processing GCC, NDVI, and GPP_{max} time series

From half-hourly GCC values, we applied a series of steps to calculate the time series of daily GCC (Luo et al., 2018), which allowed us to remove the outliers and retrieve the robust time series:

1. We discarded GCC values when PAR was below 600 μmol m^{-2} s^{-1} to filter out GCC measured during adverse meteorological conditions such as clouds or rain (Filippa et al., 2016; Migliavacca et al., 2011).
2. We extracted the 90th percentile of the GCC value from a 3-day moving window and assigned as the GCC value of the day at the center of the moving window (Sonnentag et al., 2012).
3. Daily GCC was further checked and the outliers were removed using a spline-based algorithm (Migliavacca et al., 2011; Richardson et al., 2018).

The daily maximum GPP (hereafter refers to GPP_{max}) was computed using the same procedure as the one used for GCC and using GPP data between 10 a.m. and 2 p.m. UTC.

To obtain daily NDVI data, the 16-day time series of NDVI were interpolated to daily using the spline method in the *zoo* R package (Zeileis & Grothendieck, 2005).

The resulting daily GCC, NDVI, and GPP_{max} time series were used to investigate the fertilization effects on canopy structure (GCC, NDVI) and photosynthetic capacity (GPP_{max}). Direct in situ measurements of LAI for the herbaceous layer (Melendo-Vega et al., 2018) and indirect measurements for the trees (García et al., 2015) were used to calculate ecosystem-scale LAI and compared to Landsat NDVI and GCC (Figure S3). The comparison between Landsat NDVI and observed LAI (Figure S5) indicated a good agreement.

2.3 | Extraction of seasonality metrics

Three metrics of seasonal development of vegetation activity (hereafter referred as "seasonality metrics") were extracted to determine the changes from time series of photosynthetic capacity (GPP_{max}) and canopy structure (GCC and Landsat NDVI): PTDs, for example, start of the season (SOS) and end of season; slopes during both the green-up and dry-down periods (slopes); and the amplitudes of the time series in both autumn–winter peak and in spring (amplitudes). Since the time resolution of GPP_{max} and GCC is comparable (daily), we extracted PTDs from these two time series. In contrast, although Landsat NDVI was extrapolated to daily resolution, the revisiting time of Landsat (16 days) makes it difficult to accurately describe the PTDs. Therefore, we decided to use the PTDs only from GCC and GPP. While Phenocams are robust for the determination of timing, they can be problematic for the comparison of the absolute values due to spectral calibration between individual cameras (but see Richardson, 2019). In addition, as cameras are fixed in one direction, their FOV would have some mismatches with EC footprint climatology. Therefore, we chose to use the interpolated daily Landsat NDVI to evaluate the absolute differences of amplitudes in canopy structure across sites. We also calculated slopes from NDVI time series in the green-up and dry-down phase and amplitudes of the seasonal cycle.

For the extraction of seasonality metrics time, series were first smoothed to better capture the seasonal dynamics of GCC/NDVI or GPP (Filippa et al., 2016; Migliavacca et al., 2011). PTDs, slopes, and amplitudes were extracted from the smoothed time series using the procedures described in Luo et al. (2018) and the Supporting Information (Note S1, Table S1, and Figure S4). Uncertainty of seasonality metrics was assessed by running the extraction steps repeatedly (100 times). The 100 times series were constructed by summing original data and random noise generated using the residuals between the spline-smoothed fitting and the observed data (Filippa et al., 2016).

2.4 | Water availability indexes

The time series of direct measured SWC well represent the variation of water availability in a small soil area. However, they have some

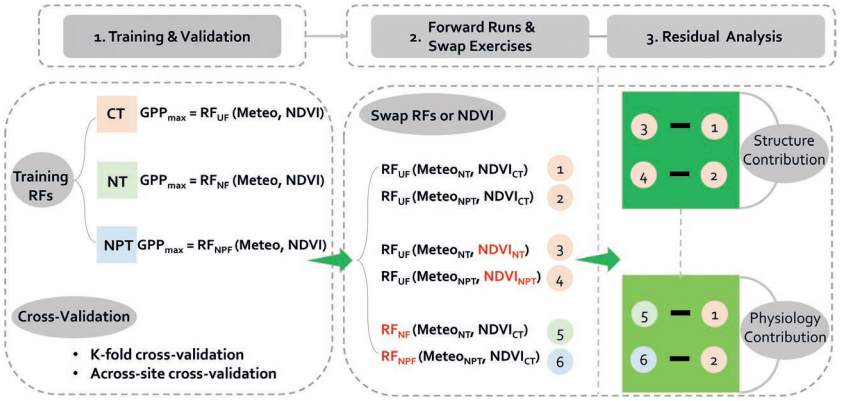

FIGURE 2 Three steps of random forest (RF) analysis. RFUF, RFNF, and RFNPF are the RF trained using the data under conditions of control, nitrogen fertilization, and nitrogen and phosphorus fertilization, respectively. The text with red color in the step of "Forward Runs & Swap Exercises" specifies the changes in RF or NDVI in each factorial model experiment. Meteo here includes both daily climate and soil water availability index. NDVI stands for the normalized difference vegetation index. For a more detailed description, readers can also refer to Note S3 and Figure S6

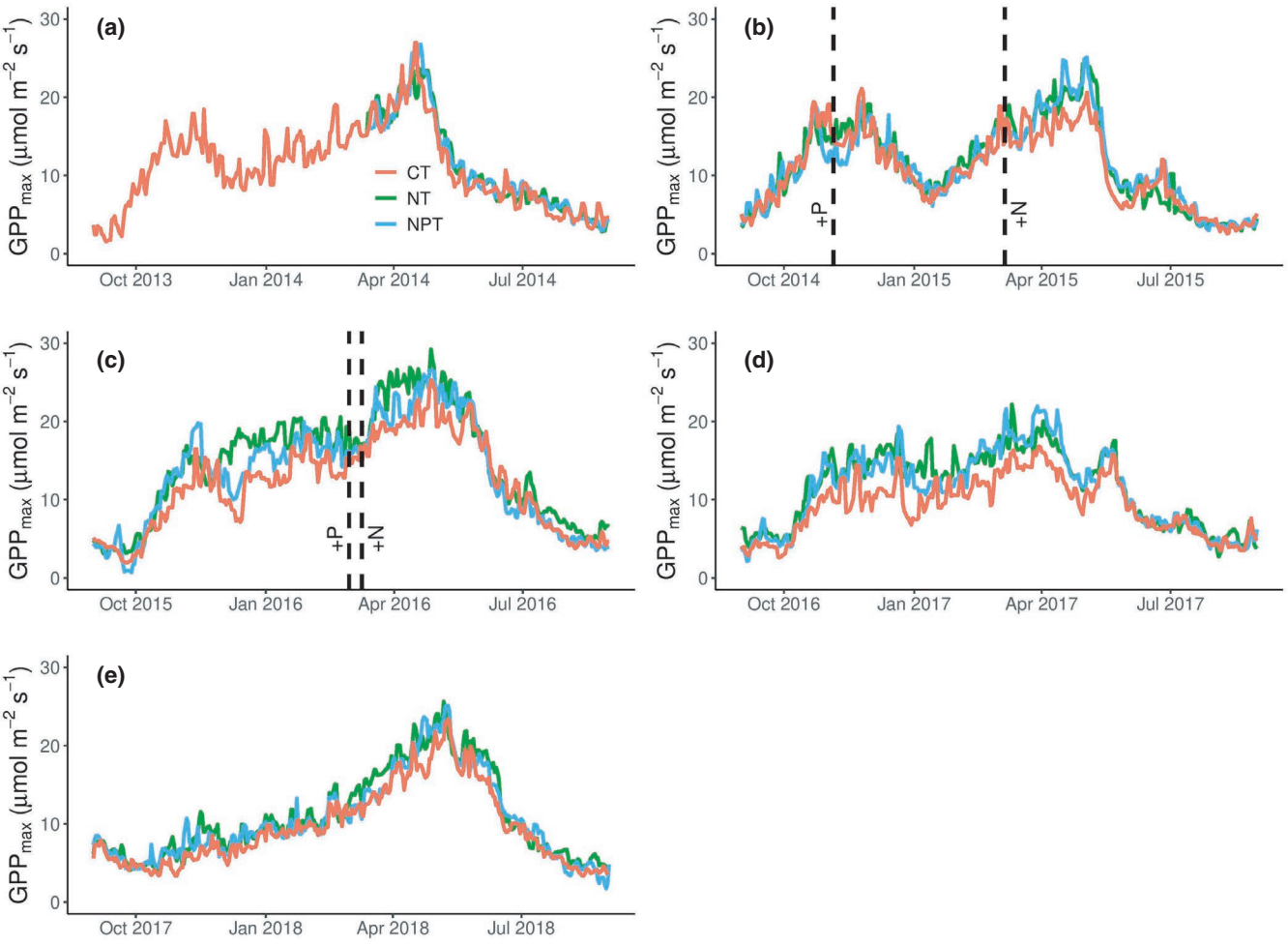

FIGURE 3 Time series of daily maximum gross primary productivity (GPP_{max}) under different fertilization treatments for the different hydrological years 2013–2017 (a–e). Control (CT), nitrogen-fertilized (NT), and nitrogen and phosphorus fertilized treatments (NPT) are in red, dark green, and light blue, respectively. The first dose of nitrogen and phosphorus fertilizers was applied in November 2014 and March 2015, respectively. The second dose was applied at the end of February and early March 2016. Fertilization dates are marked by the dashed black vertical lines

limitation for this study because (a) the spatial heterogeneity of the soil moisture is normally large (indicated by the measurements of different soil water sensors, data are not shown here), thus SWC measurements are not representing water availability well on the ecosystem scale; and (b) comparable SWC measurements among three treatments with the same setup were not available at the beginning of the experiment.

TABLE 2 Differences of phenological transition dates (PTDs), slopes, and amplitudes for photosynthetic capacity (GPP_{max}) and canopy structure (GCC/NDVI) between different fertilized treatments during green-up and dry-down periods[a,b]

	Green-up			Dry-down		
	NT-CT	NPT-CT	NPT-NT	NT-CT	NPT-CT	NPT-NT
GPP_{max}						
PTDs (day)	−0.2 ± 19.6	−0.9 ± 16.8	−1.1 ± 7.3	−19.3 ± 18.5**	−17.2 ± 18.2*	−2.1 ± 11.0
Slopes ($\mu mol\ m^{-2}\ s^{-1}\ day^{-1}$)	0.099 ± 0.026**	0.143 ± 0.053**	0.044 ± 0.040*	−0.122 ± 0.022**	−0.071 ± 0.054**	0.051 ± 0.043*
Amplitudes ($\mu mol\ m^{-2}\ s^{-1}$)	2.4 ± 0.9**	2.7 ± 1.2**	0.3 ± 1.5	n.a.[c]	n.a.	n.a.
GCC						
PTDs (day)	3.8 ± 8.0	7.3 ± 8.3	0 ± 8.0	2.2 ± 5.5	3.2 ± 5.1	0 ± 3.9
NDVI						
Slopes	(−4 ± 6) e−04	(18 ± 10) e−04**	(22 ± 9) e−04**	(−26 ± 24) e−04**	(−7 ± 6) e−04*	(−19 ± 25) e−04
Amplitudes	0.029 ± 0.027*	0.050 ± 0.046*	0.021 ± 0.056	n.a.	n.a.	n.a.

Abbreviations: GCC, green chromatic coordinate; GPP, gross primary productivity; NDVI, normalized difference vegetation index

[a]For the metrics of photosynthetic capacity, PTDs, slopes, and amplitudes were extracted from GPP_{max}. In contrast, for canopy structure, PTDs were extracted from GCC, while slopes and amplitudes were extracted from the NDVI. The differences of those metrics between pre-fertilization and post-fertilization were first calculated; the differences between treatments (Control [CT], nitrogen addition [NT], nitrogen and phosphorus addition [NPT]) were then computed. Wilcoxon test was conducted to investigate whether significant differences exist between treatments. *p* values are as follows: *.01 ≤ *p* < .05, **.001 ≤ *p* < .01. It indicated no statistically significant difference between treatments if there are no asterisks.

[b]The differences and corresponding standard errors between treatments were shown in the table (mean ± *SD*). It is noted that it means minuend has faster-decreasing speed if the difference between the two treatments is negative.

[c]All the amplitudes during green-up (Autumn–Winter) and dry-down (Spring–Summer) were used to conduct the Wilcoxon test between every two treatments. Hence, the results for the amplitudes refer to the whole season.

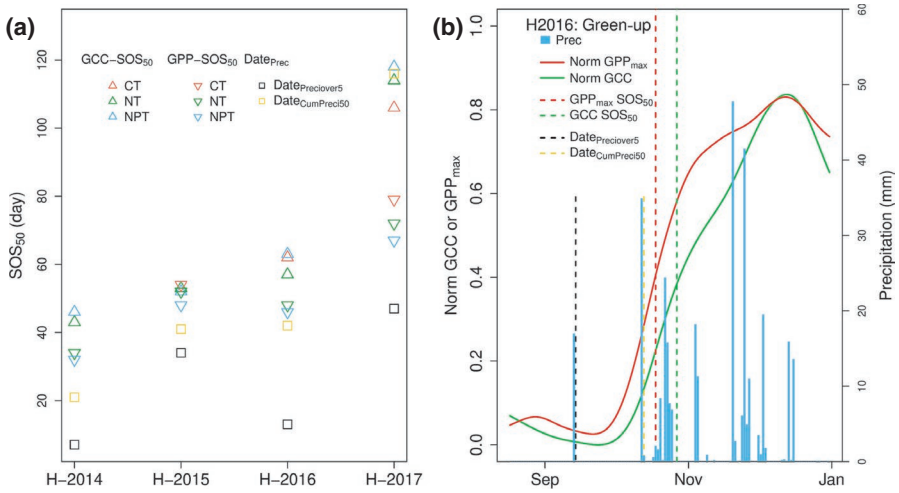

FIGURE 4 (a) Relationship between start of the season (SOS)50 and the date when daily precipitation first exceeds 5 mm (DatePreciover5) or cumulative precipitation reaches 50 mm (DateCumPreci50) in the green-up period. SOS_{50} was extracted from daily maximum gross primary productivity (GPP_{max}) or green chromatic coordinates (GCC). For the definition of SOS_{50}, readers can refer to Table S1. (b) Daily precipitation (Prec), normalized GPP_{max} or GCC in the green-up period at hydrological 2016 (H-2016) in the nitrogen-fertilized site (NT). The vertical dotted lines stand for DatePreciover5, DateCumPreci50, or SOS_{50}

Hence, we introduced soil water availability index (WAI; Tramontana et al., 2016) and conservative surface wetness index (CSWI; Nelson et al., 2018) to better represent the water availability on the ecosystem scale, which were both based on the bucket model. These indexes were preferred over SWC observations with regard to representing water availability on the ecosystem scale as they are calculated based on fluxes or meteorological variables and integrate information from large areas (the tower footprints). The half-hourly WAI and CSWI at *t* (WAI_t and $CSWI_t$) are calculated according to Equations (3) and (4), respectively:

$$WAI_t = WAI_{t-1} + R_t - ET_t, \quad (3)$$

$$CSWI_t = \max(S_t, \min(P_t, S_{max})), \quad (4)$$

where R_t and ET_t are water recharge and evapotranspiration, whereas S_t, P_t, and S_{max} are surface water storage, Prec, and maximum allowed storage (S_{max} is set to 5 mm according to the setting of Nelson et al., 2018). Readers can refer to the details of calculating WAI and CSWI in Note S2.

We used the CSWI and WAI for different purposes. The CSWI was used to study the differences in water availability between different treatments as it was calculated using measured ET in the different treatments. In contrast, we used WAI rather than CSWI as one of the environmental drivers for the random forest (RF) analysis in Section 2.5 because it is based only on meteorological data and does not used measured fluxes (i.e., ET) as input driving variables as it would be with the CSWI.

After first calculating the half-hourly WAI and CSWI, then the data during the mid-day period (10:00–14:00) were selected to be consistent with the periods of GPP_{max} and GCC/NDVI and averaged at the daily, weekly, and monthly scale to represent soil water availability for the three treatments.

To investigate how water availability influences the fertilization effects on seasonality metrics among different treatments, we calculated mean WAI during green-up and dry-down periods in each hydrological year. WAI at green-up was averaged from October to December, while WAI at dry-down was averaged during the period of May–July. Higher WAI stands for more water availability in the ecosystems.

2.5 | Disentangling the contributions from structure and physiology

The contribution of climatic and structural drivers to changes in GPP_{max} could be inferred from the time series of meteorological data and LAI (here represented by NDVI). On the contrary, the quantification of the variability in physiological response is more complex. To disentangle the contribution of structure and especially physiology to the changes of GPP_{max} after fertilization, we designed two different analyses: (a) we calculated the LUE, that is, the ratio between GPP_{max} and APAR

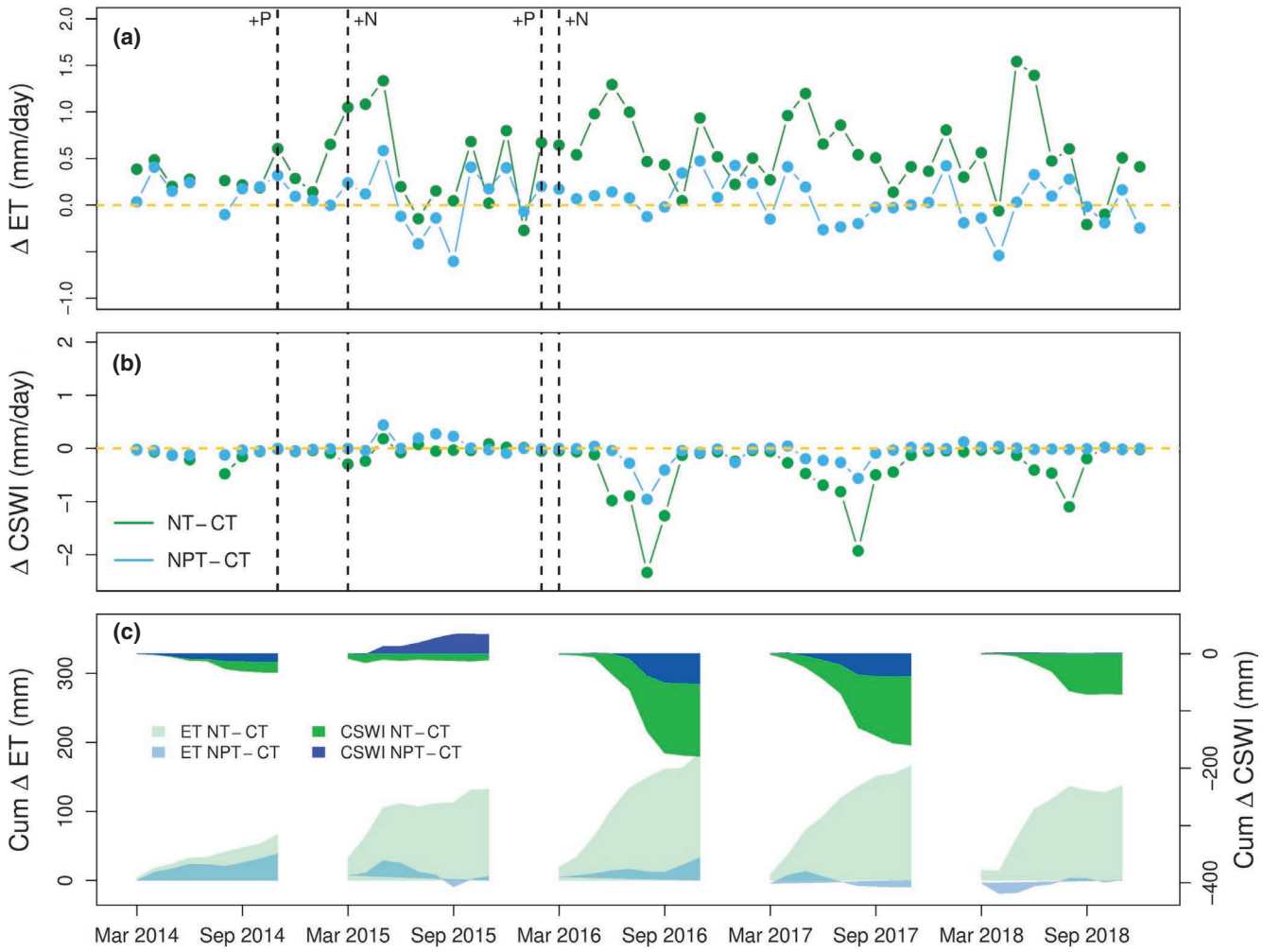

FIGURE 5 Monthly mean of differences between different treatments for (a) evapotranspiration (ET), (b) conservative surface water index (CSWI) and cumulative differences for (c) ET or CSWI at the same period in each year (March–November). Difference between treatments of nitrogen fertilized and control (NT-CT) and the difference between treatments of nitrogen and phosphorus fertilized (NPT) and CT (NPT-CT) are in green, and blue, respectively. The black vertical dotted lines represent the dates when phosphorus and nitrogen fertilizers were applied. The ET data in July 2014 were removed because of a big gap in the measurements in CT due to a lightning strike

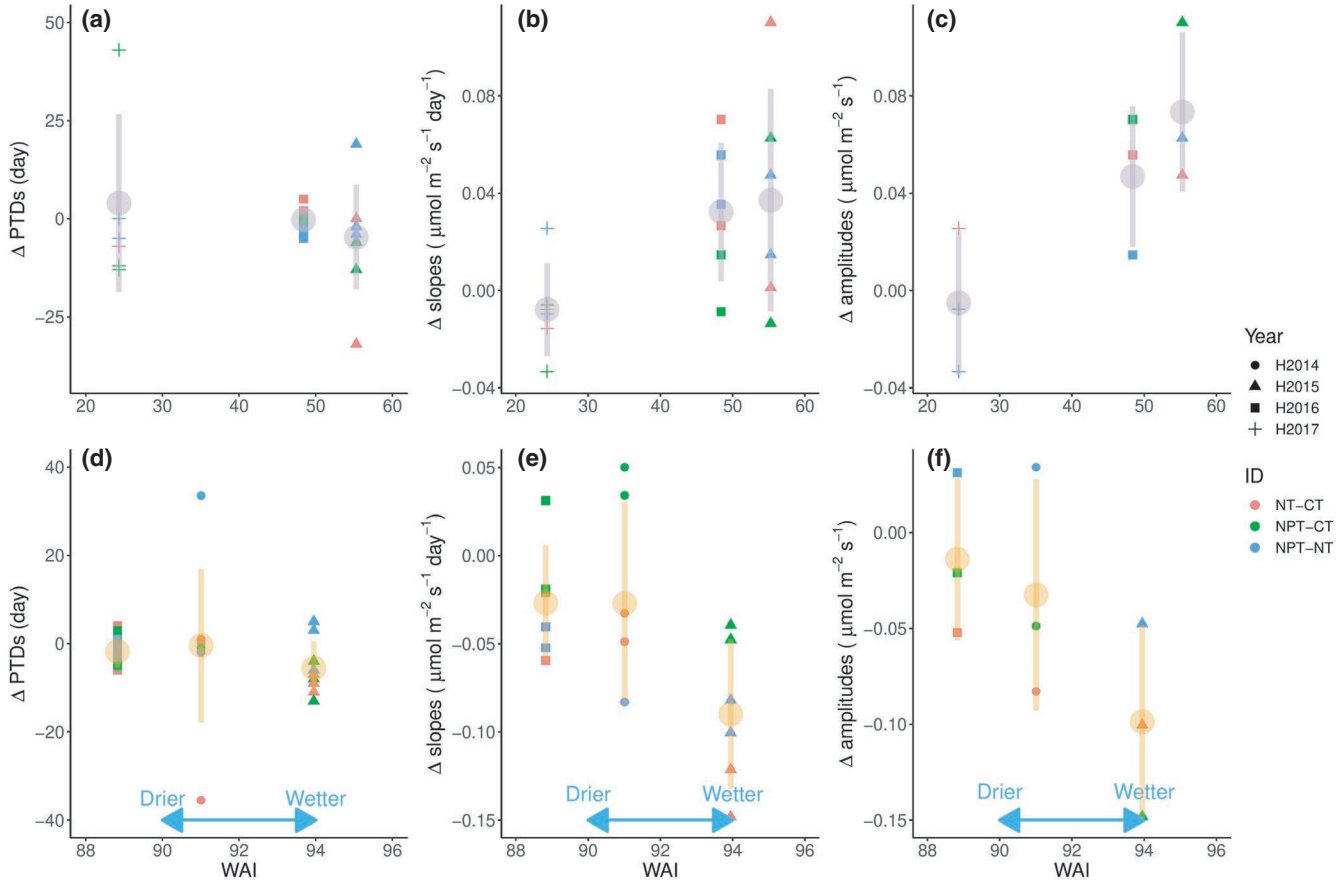

FIGURE 6 (a–c) Mean and standard deviation (*SD*) of the difference in seasonality metrics (phonological transition dates [PTDs], slopes, and amplitudes) between treatments during the green-up (a–c) and dry-down (d–f) period. Red, green, and blue stand for the differences in metrics between Control (CT) and nitrogen fertilized (NT), nitrogen and phosphorus fertilized (NPT) and CT, and NPT and NT, respectively. The gray and orange dots represent the mean difference for the same hydrological year during green-up and dry-down periods, respectively. The vertical lines stand for *SD* of differences at the same hydrological year. WAI, water availability index

derived from NDVI, with the assumptions that changes in LUE can be associated with changes in physiology induced by the fertilization; (b) we used a RF analysis to more quantitatively disentangle the contribution from structure and physiology to the changes of GPP_{max} after fertilization. Besides, RF can take different confounding factors (e.g., differences between treatments in regard to soil water availability) into consideration, which could not be considered in the LUE analysis.

2.5.1 | Light use efficiency

Light use efficiency is a physiology-related property (Reichstein, Bahn, Mahecha, Kattge, & Baldocchi, 2014) and daily LUE was calculated using Equation 5 (Monteith,1972):

$$LUE = \frac{GPP_{max}}{PAR_{max} \times fAPAR}, \quad (5)$$

$$fAPAR = 1.51 \times NDVI - 0.40, \quad (6)$$

where a fraction of absorbed photosynthetically active radiation (fAPAR) was computed by adopting a linear relationship between satellite NDVI and fAPAR in a semi-arid environment (Equation 6; Fensholt, Sandholt, & Rasmussen, 2004). Daily maximum PAR (PAR_{max}) is the PAR measured for the period retained as GPP_{max} that is described in Section 2.2.3. A significant linear regression and high correlation (r = .91) between measured green LAI and Landsat NDVI indicate that NDVI could be used to represent the green biomass absorbing radiation (Figure S5).

Daily maximum gross primary productivity, Landsat NDVI, and LUE were also averaged at different periods: that is, green-up (October–December), spring peak (March–April), dry-down (May–July), and for the whole hydrological year (H-year).

2.5.2 | RF analysis

Three main steps were applied for RF analysis (Figure 2):

1. We trained RFs using daily climate (SW_{Rad}, T_a, VPD, and day length [DL]), soil WAI, and Landsat NDVI data to predict daily GPP_{max} (i.e., ecosystem response). RFs were trained for both unfertilized (i.e., for CT) and fertilized conditions (for NT and NPT after fertilization). To evaluate the performance of RFs, we

TABLE 3 Mean of GPP_{max}, Landsat NDVI and light use efficiency (LUE) for different treatments after fertilization at different periods[a,b]

	Green-up			Dry-down			Spring peak			Hydro-year		
	CT	NT	NPT	CT	NT	NPT	CT	NT	NPT	CT	NT	NPT
GPP_{max} (μmol m^{-2} s^{-1})	9.4	11.8	11.3	10.2	11.1	11.0	15.9	18.7	18.1	10.3	12.2	11.6
Sig. (GPP_{max})		(*, ns)	(*, ns)		(ns, ns)	(ns, ns)		(*, ns)	(*, ns)		(*, *)	(*, *)
Landsat NDVI	0.54	0.60	0.60	0.43	0.47	0.48	0.64	0.70	0.72	0.52	0.57	0.58
Sig. (NDVI)		(*,*)	(*,*)		(*,*)	(*,*)		(*, ns)	(*, ns)		(*, *)	(*, *)
LUE (C mol^{-1} $PPFD^{-1}$)	4.3E−3	6.3E−3	5.9E−3	1.6E−3	2.2E−3	2.3E−3	5.1E−3	7.0E−3	7.0E−3	3.4E−3	4.8E−3	4.6E−3
Sig. (LUE)		(*,*)	(*,*)		(*, *)	(*, *)		(*, *)	(*, *)		(*, ns)	(*, ns)

Abbreviations: fAPAR, fraction of absorbed photosynthetically active radiation; GPP_{max}, daily maximum gross primary productivity; NDVI, normalized difference vegetation index; PAR, photosynthetically active radiation; PPFD, photosynthetic photon flux density

[a]LUE was calculated as the GPP_{max}/(PAR*fAPAR), where fAPAR is calculated using Landsat NDVI (see details in Section 2.4) while PAR derived from measurements from eddy covariance tower for different treatments (Control [CT], nitrogen addition [NT], nitrogen and phosphorus addition [NPT]). Mean of GPP_{max}, NDVI, and LUE after fertilization in the periods of green-up (October–December), dry-down (May–July), spring peak (March–April), and whole hydrological year (Hydro-year) were calculated.

[b]Wilcoxon test was conducted to investigate whether significant differences of GPP_{max}, NDVI, and LUE exist between treatments at different periods (for details, please refer to Section 2.6). The first sign in the brackets indicates whether there is a statistical difference between fertilized sites (NT or NPT) and unfertilized site (CT). The second one indicates whether there is a statistical difference between NT and NPT. *p* values are as follows: $^{*}p < .05$, ns for $p \geq .05$. The results at green-up and spring peak are highlighted with light green and dark green, respectively, for comparison.

conducted K-fold cross-validation (K = 10) for each treatment. Specifically, the data were randomly split into 10 subsets. Then, one subset was used for validation and the remaining subsets for training the RF. This process was repeated until each of subset had served as the validation set. The root mean squared error, R-squared (R^2), and mean absolute error in cross-validation was computed for each treatment. For unfertilized condition, 1631 data points were used for cross-validation, while 1,396 data points were used for cross-validation for N and NP fertilized condition, respectively. The very good performances of RFs in cross-validation indicated their applicability (Table S2). To evaluate the predictive capacity of the RFs across different sites before the fertilization, we trained the RFs in the CT treatment and then predicted GPP_{max} in the NT and NPT treatment during the pre-fertilized period (before November 2014). The performance of this across-site cross-validation was good ($R^2 \geq .92$) and show that the RFs are able to be predict well the GPP in a different site in the pre-fertilization phase (Figure S7), and therefore can be used to analyze the fertilization effects.

2. Then we conducted a factorial model experiment with a swap of the drivers (climate variables and Landsat NDVI) and the RFs trained in each treatment. The assumption here is that Landsat carries information on the structural change at each treatment, while the trained RFs the physiological effects (adopting similar ideas in Marcolla et al., 2011; Richardson et al., 2007). In practice, we run forward different combinations of RFs and drivers to predict GPP_{max} (Figure 2): (1) for the unfertilized condition (RF_{UF}) using the Landsat NDVI from the CT; (2) for the unfertilized condition (RF_{UF}) using the Landsat NDVI from NT and NPT (these runs account for the structural effect of fertilization on GPP_{max}); (3) for the fertilization condition (RF_{NF} and RF_{NPF}) using Landsat NDVI from the CT (these runs account for the physiological effect on GPP_{max}). At the end of this process, we obtained six time series of predicted GPP_{max} (Figure 2; Note S3).
3. An analysis of the residuals of GPP_{max} calculated between four combinations of the runs conducted at step 2 (Figure 2) was used to factor out the role of changes in physiology and structure. For example, to evaluate the structural and physiological contribution to changes in the NT treatment, we used the predicted GPP_{max} using (1) the RF trained at the CT and the NDVI of the CT tower; (2) the RF trained at the CT and the NDVI of the NT tower; and (3) the RF trained at the NT tower and the NDVI from the CT. If the residuals of GPP_{max} between (2) and (1) were higher than residuals between (3) and (1), then we concluded that changes in structure (i.e., NDVI) were the most important driver of contributors to changes in GPP_{max}. A more detailed description of methodology and procedures is found in Note S3 and Figure S6.

2.6 | Statistical analysis

We explored whether the fertilization effects were significant via conducting difference tests for the seasonality metrics derived from

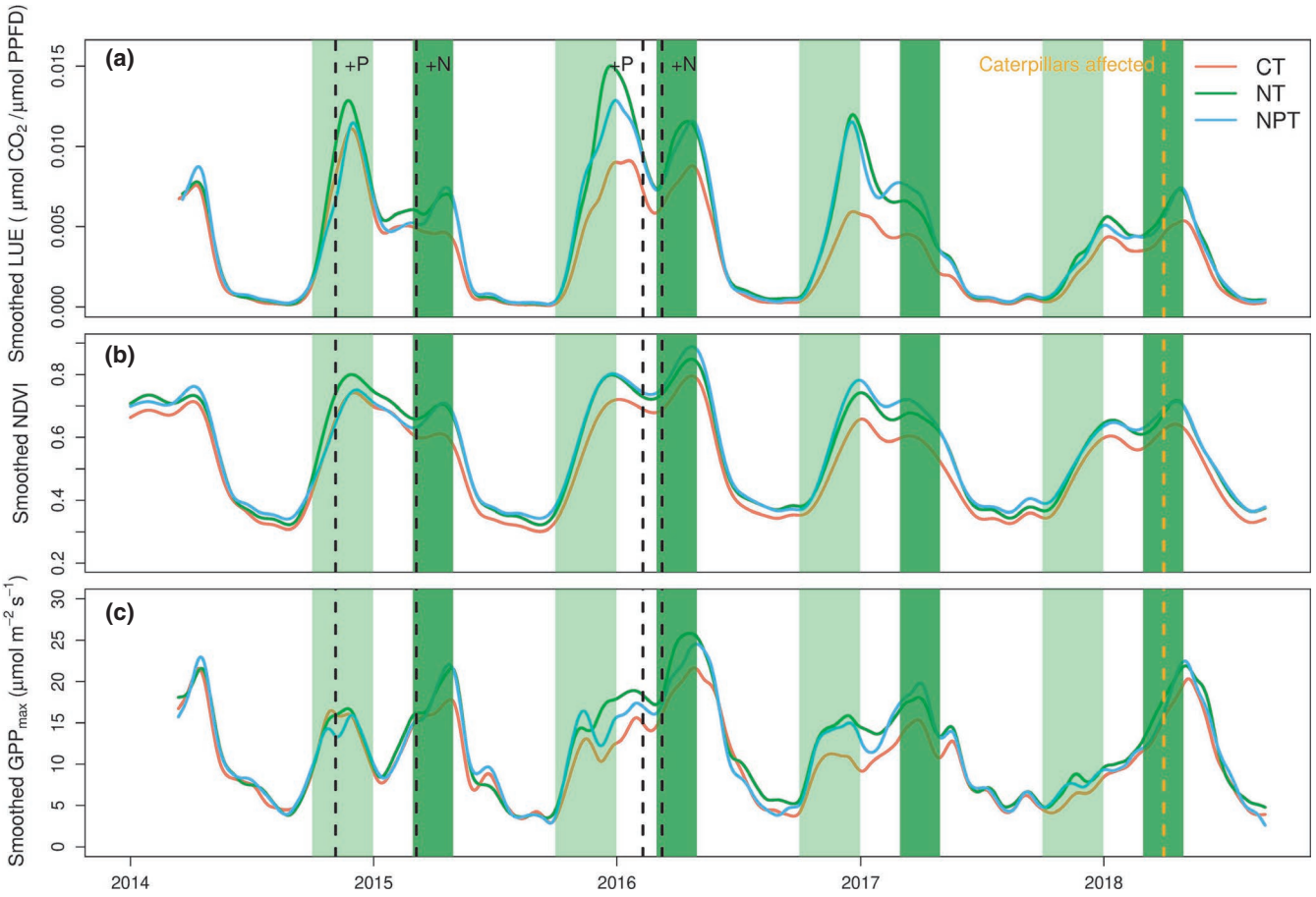

FIGURE 7 Time series of (a) smoothed light use efficiency (LUE), (b) smoothed normalized difference vegetation index (NDVI), and (c) daily maximum gross primary productivity (GPP_{max}) at Control (CT), nitrogen-fertilized (NT), and nitrogen- and phosphorus-fertilized (NPT) treatments. Periods of green-up (October–December) and spring peak (March–April) after fertilization are highlighted with light green and dark green, respectively. The black vertical dotted lines represent the dates when phosphorus and nitrogen fertilizers were applied. We also highlight the date (April 1, 2018) with an orange dotted line when trees in the experimental sites started to be attacked by caterpillars

the time series of GPP_{max}, NDVI, and GCC between different treatments. The time series of LUE in different treatments were also compared for the same reason. The difference tests applied are described below:

1. Seasonality metrics or LUE before fertilization were subtracted from the ones after fertilization. We used the differences (Δ) calculated between pre-fertilization and post-fertilization (Equation 5) to conduct statistical tests to remove the differences before fertilization among treatments (even marginally).

$$\Delta_X = X_{t_1} - X_{t_0}. \quad (7)$$

In Equation (7), X represents metrics or LUE, while t_1 and t_0 stand for the post-fertilization and pre-fertilization, respectively.

1. The differences between every two treatments (Δ_{X_T}, i.e., NT − CT, NPT − CT, and NPT − NT) were then calculated and a Wilcoxon test was applied to investigate whether the differences are significant or not among different treatments. Please refer to Note S4 for the details of difference tests for different metrics or LUE.

$$\Delta_{X_T} = \Delta_{X_{T1}} - \Delta_{X_{T2}}. \quad (8)$$

In Equation (8), Δ_{X_T} stands for the differences of Δ calculated in step 1, between every two treatments. $T1$ and $T2$ stand for two different treatments of three, respectively.

3 | RESULTS

3.1 | Fertilization effects on seasonality of photosynthetic capacity and canopy structure

Daily maximum gross primary productivity of the three treatments was similar before the fertilization (before November 2014), and the differences between fertilized (NT and NPT) and unfertilized sites (CT) started to be significant after N fertilization in March 2015 (Figure 3). The differences between treatments

also showed large interannual variability. For instance, in the hydrological year 2016 (i.e., H2016: September 2016–August 2017, where Prec was 65 mm above the mean Prec; 12% increase compared to mean), there were large differences between treatments. In the hydrological year 2017 (H2017), when the rainfall was quite low in the autumn and winter seasons (229 mm less rainfall, i.e., 53% decrease) compared to the historical mean for the same period), the differences of GPP_{max} between treatments became smaller.

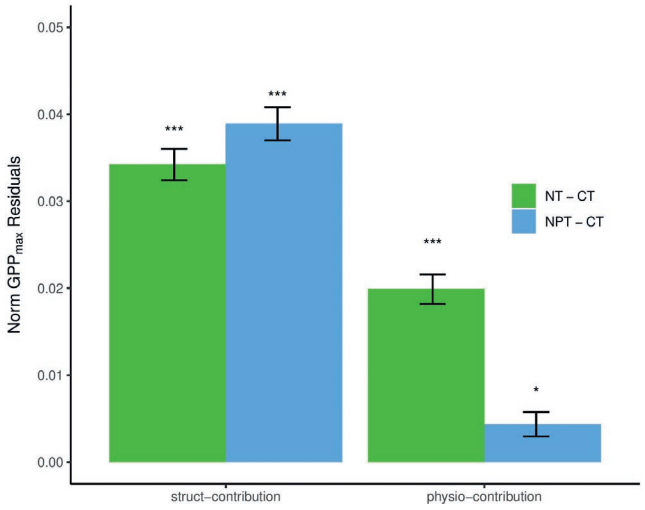

FIGURE 8 Contribution from the structure (struct-) and physiological factors (physio-) to the changes in normalized daily maximum gross primary productivity (GPP_{max}) after fertilization from random forest analysis. The mean difference between nitrogen fertilized (NT) and Control (CT) and the mean difference between nitrogen and phosphorus fertilized (NPT) and CT are displayed. The error bars represent standard errors. Significant differences were determined by the Wilcoxon test. *p*-values are as follows: *.01 ≤ *p* < .05, ***p* < .001. Note that struct- contribution is adjusted by subtracting the differences between NT − NPT and CT before fertilization

Differences among treatments were also observed for metrics derived from GPP_{max} (Table 2; Figure S8). For PTDs, there were no differences between treatments at green-up, while in both NT and NPT senescence started earlier (17–19 days) than at CT in the dry-down period. Both NT and NPT GPP_{max} showed faster green-up (with slopes being 0.10 ± 0.03 (mean ± *SD*) and 0.14 ± 0.05 μmol m^{-2} s^{-1} day^{-1} higher than CT, respectively) and faster dry-down (0.12 ± 0.02 and 0.07 ± 0.05 μmol m^{-2} s^{-1} day^{-1} lower than CT, respectively). Within fertilized treatments, NPT had a significantly faster increase in GPP_{max} in the green-up period, and a slower decrease in GPP_{max} at dry-down compared to NT. Regarding the amplitudes, NT and NPT had significantly higher amplitudes compared to CT, while there was no significant difference between NT and NPT (Table 2).

The canopy structure also differed among treatments (Table 2). The PTDs extracted from GCC showed no significant differences between treatments both during green-up and dry-down periods. Fertilized sites (NT and NPT) generally had faster changes of NDVI compared to CT. However, there were no significant differences between NT and CT at green-up and between NPT and NT in the dry-down period. Similar to GPP_{max}, amplitudes of NDVI in NT and NPT were significantly higher than in CT.

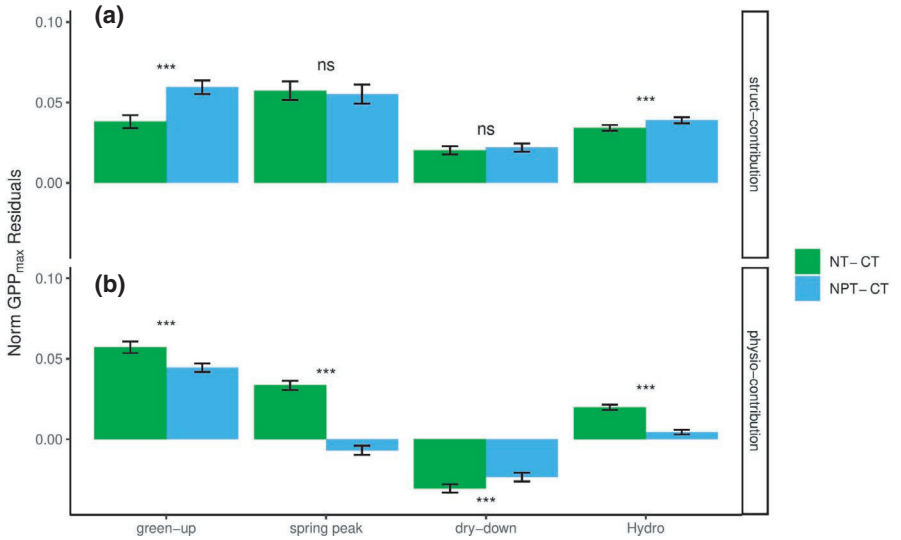

FIGURE 9 Contribution from changes in (a) structure (struct-) and (b) physiological factors (physio-) to the changes in normalized GPP_{max} after fertilization at different periods from random forest analysis. Mean difference and standard error between fertilized sites (nitrogen fertilized: NT or nitrogen and phosphorus fertilized: NPT) and Control (CT) at periods of green-up (October–December), dry-down (May–July), spring peak (March–April), and the whole hydrological year (Hydro-year) were calculated and presented. The differences between NT − NPT and CT are all statistically significant different. The statistical differences between NT and NPT were also tested and the signs of statistical test are shown. *p*-Values are as follows: ns: *p* ≥ .05, ***p* < .001. Note that struct- contribution is adjusted by subtracting the differences between NT − NPT and CT before fertilization

3.2 | Relationship between water availability and fertilization effects

3.2.1 | Relationship between Prec and PTDs during green-up period

The relationship between Prec and the PTD SOS_{50} (the timing when reaching 50% of the amplitude of GPP_{max}, details in Table S1) extracted from GCC or GPP was investigated (Figure 4; Figure S9). SOS_{50} was more strongly related to the date when cumulative Prec reached 50 mm ($Date_{CumPreci50}$) than to the date of Prec onset, that is, when daily Prec first exceeds 5 mm ($Date_{Preciover5}$; Figure 4). For instance, in H2016, even though one large rainfall event occurred quite early, the onset of the green-up occurred late and was more related to $Date_{CumPerci50}$ (Figure 4b).

3.2.2 | Differences of ET and soil water availability between different treatments

The monthly mean of differences of ET and soil water availability between two fertilized sites (NT and NPT) and control, as well as their cumulative differences, were investigated to understand how fertilization affected water availability (Figure 5). The results showed that NT had larger cumulative ET compared to CT, and the differences between them were largest during the spring (65.7 mm) and early summer (49.1 mm). The calculated monthly CSWI shows the NT treatment had lower water variability compared to CT and the largest difference (−0.71 mm/day) occurs in the summer period (Figure 5b). The cumulative differences of ET and CSWI (Figure 5c) between NT and CT were higher after fertilization, which is consistent with the trend observed in SWC data (Figure S12).

Compared to the differences between NT and CT (0.51 mm/day), the monthly mean differences of ET between NPT and CT (0.06 mm/day) were much smaller (Figure 5a). Likewise, from monthly mean CSWI (Figure 5), the differences between NPT and CT were much smaller compared to the difference between NT and CT (e.g., −1.4 mm/month between NPT and CT, while −10.1 mm/month between NT and CT). This pattern was also observed from the measured SWC; SWC in NPT was similar to that in CT (Figure S12). The cumulative difference of ET showed NPT used a slightly larger amount of water compared to CT (difference of 18.9 mm/year) for ET, in contrast with a much larger difference between NT and CT (137.2 mm/year). The cumulative CSWI also indicated the difference in water availability between CT and NPT was much smaller compared to the difference between CT and NT (Figure 5).

3.2.3 | Interannual differences of seasonality metrics between treatments

The differences in seasonality metrics between treatments for different water availability levels are displayed in Figure 6. With the exception of the differences of PTDs during the green-up period, the differences of metrics between treatments were larger with the increase in water availability (higher WAI). At green-up, with WAI increased from 24.3 (in H2017) to 55.3 (in H2015), the mean difference of slopes between treatments increased from −0.008 ± 0.019 to 0.037 ± 0.046 μmol m^{-2} s^{-1} day^{-1}. Likewise, the mean difference of amplitudes between treatments increased from −0.005 ± 0.030 to 0.07 ± 0.033 μmol m^{-2} s^{-1}. In the dry-down period, the WAI of different hydrological years changed within a small range (from 88.8 at H2016 to 93.9 at H2015). However, we can clearly observe that the absolute differences of seasonality metrics between treatments increased with the increase in WAI. The mean difference for slopes increased from −0.027 ± 0.033 (H2016) to −0.090 ± 0.042 μmol m^{-2} s^{-1} day^{-1} (H2015), while the mean absolute differences for amplitudes increased from 0.014 ± 0.042 (H2016) to 0.098 ± 0.050 μmol m^{-2} s^{-1} (H2015). Even with larger variation and more uncertainty, there was a similar trend for mean difference for PTDs between treatments in the dry-down period (ranges from −0.4 ± 17.3 to −5.6 ± 6.0 day).

3.3 | Contribution of structure and physiology to the changes of GPP_{max}

3.3.1 | Comparison of GPP_{max}, NDVI, and LUE between treatments at different periods

In general, the fertilized treatments (NT and NPT) had higher GPP_{max} in all periods (Table 3). They were especially significantly higher during the green-up (the differences are 2.4 ± 0.14 [mean ± *SE*] μmol m^{-2} s^{-1} between NT and CT, and 1.9 ± 0.11 μmol m^{-2} s^{-1} between NPT and CT, respectively) and the spring peak (the differences are 2.9 ± 0.13 μmol m^{-2} s^{-1} between NT and CT, and 2.3 ± 0.15 μmol m^{-2} s^{-1} between NPT and CT, respectively). Within fertilized treatments, NT had a slightly higher GPP_{max} but was not significantly different from NPT. Likewise, the NDVI in NT and NPT was significantly higher than NDVI in CT (difference of NDVI is 0.05 ± 0.001 between NT and CT, and 0.06 ± 0.001 between NPT and CT, respectively). The NDVI of NPT was slightly higher than in NT with the highest NDVI observed at the spring peak (0.72 ± 0.005).

After fertilization, LUE increased significantly both at NT and NPT compared to CT (Figure 7; Table 3), and this increase was most prominent in the green-up period (mean ± *SE*: 0.0020 ± 0.0001) when compared to NT and CT, and 0.0016 ± 0.0001 when compared NPT and CT, respectively; Figure 7). Moreover, apart from H2017 (with very dry autumn and winter), the LUE was highest in the green-up period even if a lower NDVI was observed at this time compared to spring peak (Figure 7).

3.3.2 | Results of RF analysis

The results of the RF analysis showed that most of the contribution to the changes of GPP_{max} in the fertilized treatments can be

attributed to changes in structure (Figure 8). In the NT, both structure and physiology contributed to changes in GPP_{max}, while in NPT structure was the main driver.

Contributions to the variation of GPP_{max} from physiology and structure varied during the year (Figure 9; Figure S14). Consistent with LUE analysis, the RF analysis showed the most prominent contribution from physiology occurred at green-up, while structure both contributed largely at green-up and spring peak (Figure 9). In the dry-down period, contributions from the structure (positive contribution) and physiology (negative contribution) to the increase in GPP_{max} were divergent, which resulted in the lowest total contribution to GPP_{max} (Figure 9; Figure S14).

4 | DISCUSSION

The overall fertilization effects on GPP_{max} and the contribution from structure and physiology to changes of GPP_{max} are summarized as the schematic plot in Figure 10.

4.1 | Water and nutrients are co-mediating the seasonality of vegetation activity

In this part, we discuss the factors driving the photosynthetic capacity as described in Figure 10, and the interactions between nutrients and water availability. We focus on the phenology in the green-up, dry-down periods, and the variation of GPP_{max} amplitudes and the interannual variability. Specifically, the timing of green-up is solely controlled by Prec; the speed of green-up and amplitudes are modulated by the combination of water and nutrients; the earlier and faster senescence in fertilized sites are related to the water limitation and species changes; higher water availability amplifies the nutrients' effects on GPP_{max}.

4.1.1 | Onset of green-up period: Prec is the controller of timing of green-up

Precipitation determines the timing of green-up and the onset of photosynthetic activity (Figure 4). As the greenness of evergreen oak

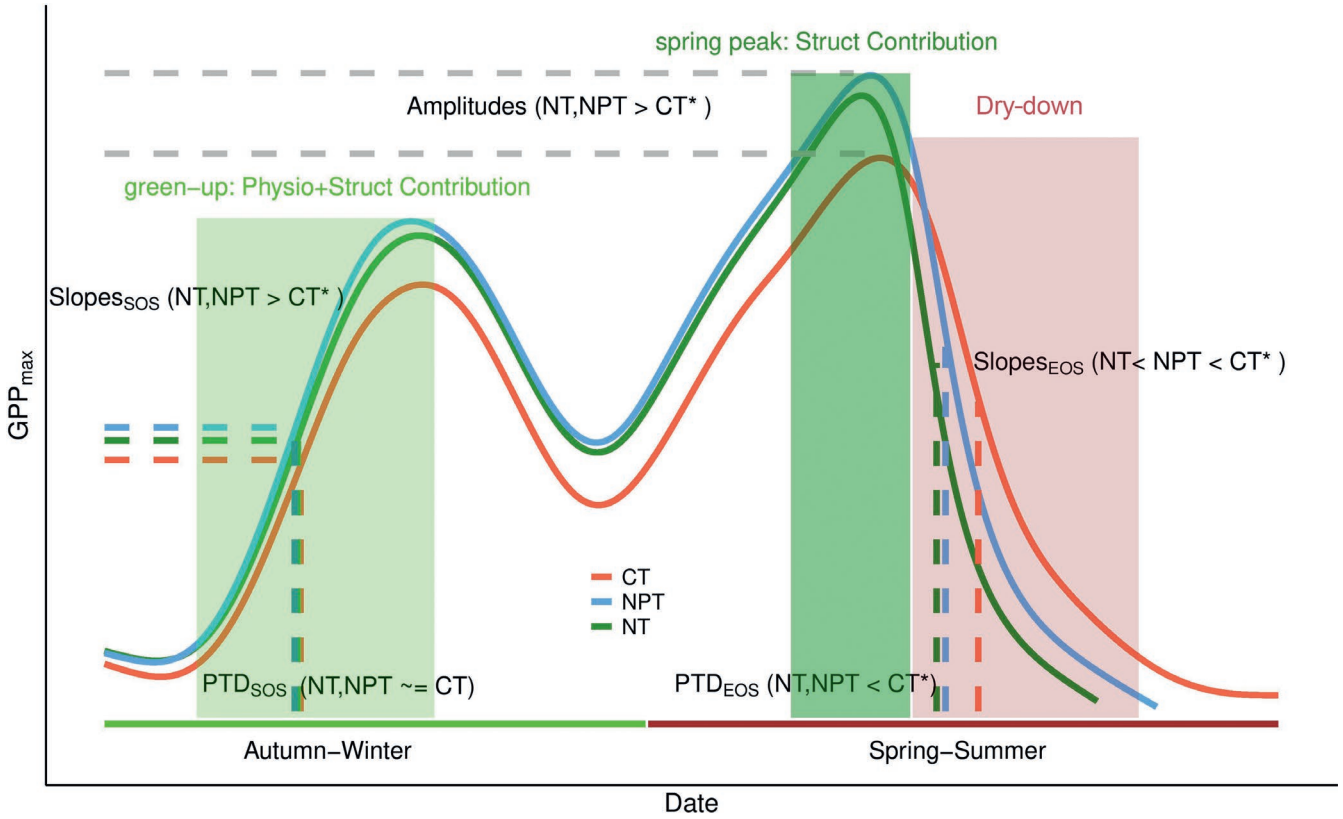

FIGURE 10 General illustration of fertilization effects on photosynthetic capacity (daily maximum gross primary productivity [GPP_{max}]). Control (CT), nitrogen-fertilized (NT), and nitrogen- and phosphorus-fertilized treatments (NPT) are in red, dark green, and light blue, respectively. Three different categories of seasonality metrics (phenological transition dates [PTDs], slopes, and amplitudes) were used to evaluate the fertilization effects. The symbol "*" indicates statistically significant differences between treatments. Note that the symbol "<" for comparison of slopes during the dry-down indicated the faster speed of senescence (more negative value). The periods of green-up, spring peak, and dry-down were indicated by light green, dark green, and light brown, respectively. Physiological factors (Physio) mainly contribute to the increase in GPP_{max} in the green-up period, while structure (Struct) contributes to the increase in GPP_{max} both at green-up and spring peak. EOS, start of the season; SOS, end of the season

trees remains relatively constant during the green-up period, the timing of green-up at the ecosystem scale is therefore mainly determined by the herbaceous layer (Luo et al., 2018). Some studies conducted on semi-arid regions in North America, Africa, and Europe (Gong, Fanselow, Dittert, Taube, & Lin, 2015; Jolly & Running, 2004; Kurc & Benton, 2010) showed that the onset of green-up is initialized by the Prec, which is in agreement with our results (Figure S11, green-up is initialized by certain amount of rainfall), while other studies suggest a widespread pre-rainfall vegetation green-up in Africa (Adole, Dash, & Atkinson, 2018). After warm and dry summer, soil moisture especially that in the top soil layers, drops to levels unsuitable for the growth of herbaceous plants (Jolly & Running, 2004; Xu, Medvigy, Powers, Becknell, & Guan, 2016). With the onset of rainfall in autumn, soil moisture increases and grasses start to invigorate once water transport through the roots could sustain the turgor for biological activities in leaves (Condit et al., 2000; Hsiao, 1973). However, we show that the onset of the vegetation occurs not immediately after the first major Prec event, but once cumulative Prec reaches a certain amount, namely c.a. 50 mm (Figure 4). This is possible because both the frequency and intensity of Prec can influence the growth of vegetation (Rishmawi, Prince, & Xue, 2016; Svoray & Karnieli, 2011) through changing soil water availability. One single Prec event could not always provide a water pulse sufficient to trigger the start of green-up or ecosystem productivity (Reynolds, Kemp, Ogle, & Fernández, 2004). By comparing our 4-year record of daily rainfall and SWC in the green-up period (Figure S11), we found that vegetation becomes active when the SWC in the top 20 cm is around or exceeds 20%.

4.1.2 | Increased speed of green-up and amplitudes due to larger resources usage or higher resource use efficiency

N and NP fertilization result in a faster increase in GPP_{max} during the green-up period and higher amplitudes of GPP_{max} in fertilized sites (Table 2; Figure S9). With increasing Prec and soil water availability in early autumn (Figure S11), more organic and inorganic nutrients are accessible to plants (Agehara & Warncke, 2005; Zhang & Wienhold, 2002). Previous leaf biophysical and biochemical measurements indicate that leaves rapidly expand and pigments linearly increase in the green-up period (Croft, Chen, Froelich, Chen, & Staebler, 2015; Yang, Tang, & Mustard, 2014). With higher availability of nutrients and observed higher root biomass and root length density in fertilized sites (Nair et al., 2019), nutrients like N can be absorbed and used for leaves. In the study site, increasing N in leaf pools and increases in specific leaf area were observed (Nair et al., 2019). These increases cause a rise in the maximum carboxylation rate (V_{cmax}) and chlorophyll (Pacheco-Labrador et al., 2019). As a result, the photosynthetic capacity would increase (Fleischer et al., 2013; Tatarko, 2017), which likely contributes to the faster increase in GPP_{max} and biomass (as demonstrated by NDVI) in the fertilized treatments in the green-up period (Table 2). At the same time, with higher total amount of nitrogen, fertilized sites were observed having higher LAI, which contributes to the notably higher amplitude of GPP_{max} and NDVI in NT and NPT (Table 2). This is consistent with the current understanding of nutrient addition that results in increased biomass (Tilman, 1987) and productivity (Guo, Hu, et al., 2016; LeBauer & Treseder, 2008).

During the growing season, soil water availability supports the growth of plants (Grossiord et al., 2017; Meza, Montes, Bravo-Martínez, Serrano-Ortiz, & Kowalski, 2018). Compared to CT, more water usage in NT results in larger LE fluxes (i.e., higher ET; Figure 5). Accompanied with high nutrient availability, higher GPP capacity occurs in NT, which conforms the phenomenon observed in previous studies that higher availability of water and nitrogen induce the higher ecosystem productivity (Harpole, Potts, & Suding, 2007; Niu et al., 2009; Wang et al., 2012). In contrast, NPT uses a similar amount of water than CT (Figure S12; Figure 5) while sustaining similar GPP_{max} and even slightly higher greenness than NT (Table 2). This is might due to enhanced water use efficiency observed at the NPT site, which is supported by observation on stable carbon isotope signature (δ^{13} C) measured in a fully factorial N and P manipulation of the herbaceous layer of the site (Martini et al., 2019). Therefore, the faster green-up and increased amplitudes in the fertilized sites could either result from larger resource utilization (NT) or from improved resource use efficiency (NPT).

4.1.3 | Earlier and faster senescence in fertilized sites related to larger water usage and species changes

During the dry-down period (May–July), SWC drops dramatically on the topsoil layers due to increasing ET with the rise of air temperature and scarce rainfall (Battista et al., 2018; Luo et al., 2018; Montaldo, Albertson, & Mancini, 2008). Under these circumstances, faster usage of water in the NT accelerates the decrease in SWC on the topsoil (Figure S11) and furtherly hampers the photosynthesis once the SWC drops below certain amounts (Sardans & Peñuelas, 2013). The resulting water scarcity will induce significant response of plant, for example, decrease in green LAI (El-Madany et al., 2018; Xu & Baldocchi, 2004), and altered root depth profiles (Nair et al., 2019), producing oxidative stress-related compounds (Hernández, Alegre, & Munné-Bosch, 2004; Sardans & Peñuelas, 2013) and reducing metabolic activity (Rivas-Ubach, Sardans, Pérez-Trujillo, Estiarte, & Peñuelas, 2012; Sardans & Peñuelas, 2013). This will result in earlier and faster senescence (Chen, Wang, Xiong, Cao, & Deng, 2015; Pic, de La Serve, Tardieu, & Turc, 2002), which was observed in NT.

Moreover, fertilization can induce changes in species diversity (Isbell et al., 2013; Soons et al., 2017) and N fertilization is likely to select early-senescing species (Wang & Tang, 2019). Several species surveys were conducted within the PhenoCam FOV between the peak of the season and the dry-down period in 2017–2018. The results show, with approaching the end of dry-down, the abundance of forbs was lower in the fertilized sites compared to unfertilized sites in 2018 (this phenomenon was also observed in the first year of a factorial nutrient fertilization experiment conducted in the

same area; Martini et al., 2019; Migliavacca et al., 2017; Perez-Priego et al., 2015) and this was most significant in the NPT treatment (Figure S13). As the forbs are generally the latest senesced during the dry-down (G. Moreno, personal communication), the decrease in abundance of forbs in fertilized sites in the dry-down period might lead to earlier senescence and yellowing in fertilized sites (Table 2; Figure 10). However, the different phenomenon in NT for 2017 and 2018 indicates the question might be more complicated and needs further investigation.

4.1.4 | Interannual variability of fertilization effect is modulated by water availability

The effect of the different treatments on GPP_{max} seasonal course and seasonality metrics (PTDs, slopes, and amplitudes) is enhanced in years with higher water availability (Figures 3 and 6). Apart from the amount of N added, the response of biomass and productivity of the ecosystem to exogenous N can also depend on the intensity of rainfall (Guo, Hu, et al., 2016; Lee, Manning, Rist, Power, & Marsh, 2010). With increasing amounts of Prec in rainfall events, N-induced stimulation of GPP_{max} can be the main contributor to the increase in total GPP (Guo, Hu, et al., 2016; Guo, Li, et al., 2016). This is because the low availability of water might prevent added N from becoming biologically available (Agehara & Warncke, 2005; Lee et al., 2010). Hence, with increased soil water availability, plants can utilize more nutrients to synthesize biomass (Lee et al., 2010), and enlarged differences between fertilized and unfertilized sites are observed (Figure 5). Effects of amounts of Prec on ecosystem function should be further explored to identify the relationship between Prec and ecosystem response and its interaction with nutrient availability more clearly (Harper, Blair, Fay, Knapp, & Carlisle, 2005; Huxman et al., 2004; Rishmawi et al., 2016).

4.2 | Contribution of physiology and structure to the variation of GPP_{max}

4.2.1 | Temporal variability

During the green-up, the changes of GPP_{max} values are mainly attributed to the changes in the physiology and canopy structure. In contrast, the changes of GPP_{max} in the spring peak are mainly attributed to the changes in structure (Figure 9). The analysis of LUE also confirms the results from the RF modeling. The largest increases in LUE (physiologically related index) in fertilized sites took place during the green-up period (Figure 7). Lower LUE but higher GPP_{max} at the peak of the season (Figure 7; Table 3) indicates the larger contribution from the structure (i.e., NDVI, as a proxy of LAI and biomass) at this period (Figure S5). In the green-up period, with more nutrients available at fertilized sites, LAI and chlorophyll increase simultaneously, hence both structure and physiology contribute to the increase in GPP_{max}. At spring peak, leaves are matured and the total concentration of chlorophyll stays constant or even declines gradually (Gitelson, Viña, Ciganda, Rundquist, & Arkebauer, 2005; Yang et al., 2014). In contrast, LAI generally stabilizes along the whole peak period (Croft et al., 2015). Therefore, compared to the green-up period, the contribution from physiology to the increase in GPP_{max} is decreasing and the main contribution can be ascribed to LAI. With absolute higher LAI after fertilization (Albaugh, Allen, Dougherty, Kress, & King, 1998; Gong et al., 2015), GPP_{max} increased most at fertilized sites in spring peak compared to other periods (Table 2).

4.2.2 | Variability between treatments

Increased GPP_{max} is mainly driven by structural changes both in NT and NPT while physiology contributes to the additional increase in GPP_{max}, in particular in NT (Figure 7). The increase in N availability in fertilized sites might promote more synthesis of chlorophyll (Fleischer et al., 2013; Schlemmer, Francis, Shanahan, & Schepers, 2005) that stimulates the photosynthetic activities and increases GPP_{max} (Figure 3) in NT and NPT. However, the different availability of phosphorus in these two treatments might exert different ecosystem responses. The nitrogen-only addition in NT results in higher N:P ratio in plants (Nair et al., 2019), which might change the ratio of RNA to proteins in plants (Loladze & Elser, 2011; Peñuelas et al., 2013), potentially producing more photosynthesis-related proteins (Matzek & Vitousek, 2009), which then contributes to more increase in GPP_{max} compared to NPTcom (especially at peak of season when they have the largest difference). A recent review related to molecular mechanism of N–P interplay in plants (Hu & Chu, 2019) points that high availability of N and P like in NPT can moderately stimulate the growth of plants, and the N- and P-related gene expression. However, only with high availability of N while simultaneously lacking P, plants tend to strongly activate the nitrate responsive and phosphate starvation-induced genes, which intensifies the utilization of nitrate and limiting phosphate in plants (Hu & Chu, 2019). This may explain the higher contribution of physiology to NT in the green-up period. On the other hand, in the dry-down period, earlier and faster senescence in the fertilized sites (Figure 10) consequently results in fewer physiological contributions to the increase in GPP_{max} compared to CT (Figure 9).

4.3 | Implication of this study for global change ecology

Here we show that the interaction of availability of nutrients and water influences canopy structure and photosynthetic capacity. Water availability not only has an important influence on the timing of green-up but also modulates the effects of nutrients on the magnitudes of photosynthetic capacity response. At the same time, N addition also tends to deplete water faster in the spring peak and dry-down periods, which advances and accelerates the dry-down.

This response is alleviated with N:P ratio recovering after adding P into ecosystem (Table 2). These interactions between nutrients and water availability further draw more attention to the compensation effects of nitrogen addition on carbon budgets. Namely, the positive feedbacks of ecosystem productivity to nutrients addition at green-up and peak of the season may be offset by the decrease in carbon uptake during the dry-down period in water-limited ecosystems. With projected continuous global warming (Diffenbaugh, Swain, & Touma, 2015; Intergovernmental Panel on Climate Change, 2013) and the increase in regional drought (Mazdiyasni & AghaKouchak, 2015; Zhou, Zhang, Park Williams, & Gentine, 2019), compensation effects are expected to be intensified when growing season length is shortened with decreasing water availability (Ma, Huete, Moran, Ponce-Campos, & Eamus, 2015). We therefore advocate for more attention on changes of seasonality of canopy development and ecosystem carbon fluxes, how changes in plants water usage interacts with nutrients availability and N:P stoichiometry in seasonally dry ecosystems.

ACKNOWLEDGEMENTS

The authors acknowledge the Alexander von Humboldt Foundation for supporting this research with the Max-Planck Prize to Markus Reichstein. Yunpeng Luo and Mirco Migliavacca gratefully acknowledge financial support from the China Scholarship Council. Gerardo Moreno acknowledges financial support from the grant agreement IB16185 of the Regional Government of Extremadura.

DATA AVAILABILITY STATEMENT

The data that support the findings of this study are available from the corresponding author upon reasonable request.

ORCID

Yunpeng Luo https://orcid.org/0000-0001-6383-8300
Gianluca Filippa https://orcid.org/0000-0002-4554-6045
Solveig F. Bucher https://orcid.org/0000-0002-2303-4583
Yonatan Cáceres Escudero https://orcid.org/0000-0002-3015-6968

REFERENCES

Adole, T., Dash, J., & Atkinson, P. M. (2018). Large-scale prerain vegetation green-up across Africa. *Global Change Biology*, *24*(9), 4054–4068. https://doi.org/10.1111/gcb.14310

Agehara, S., & Warncke, D. (2005). Soil moisture and temperature effects on nitrogen release from organic nitrogen sources. *Soil Science Society of America Journal*, *69*(6), 1844–1855. https://doi.org/10.2136/sssaj2004.0361

Ahlstrom, A., Raupach, M. R., Schurgers, G., Smith, B., Arneth, A., Jung, M., … Zeng, N. (2015). The dominant role of semi-arid ecosystems in the trend and variability of the land CO_2 sink. *Science*, *348*(6237), 895–899. https://doi.org/10.1126/science.aaa1668

Albaugh, T. J., Allen, H. L., Dougherty, P. M., Kress, L. W., & King, J. S. (1998). Leaf area and above- and belowground growth responses of loblolly pine to nutrient and water additions. *Forest Science*, *44*(2), 317–328. https://doi.org/10.1093/forestscience/44.2.317

Battista, P., Chiesi, M., Fibbi, L., Gardin, L., Rapi, B., Romanelli, S., … Maselli, F. (2018). Simulation of soil water content in Mediterranean ecosystems by biogeochemical and remote sensing models. *Water*, *10*(5), 665. https://doi.org/10.3390/w10050665

Beer, C., Reichstein, M., Tomelleri, E., Ciais, P., Jung, M., Carvalhais, N., … Papale, D. (2010). Terrestrial gross carbon dioxide uptake: Global distribution and covariation with climate. *Science*, *329*(5993), 834–838. https://doi.org/10.1126/science.1184984

Bloom, A. J., Chapin, F. S., & Mooney, H. A. (1985). Resource limitation in plants – An economic analogy. *Annual Review of Ecology and Systematics*, *16*, 363–392. https://doi.org/10.1146/annurev.es.16.110185.002051

Burner, D. M., Brauer, D. K., Snider, J. L., Harrington, C. A., & Moore, P. A. (2014). Phenological responses of juvenile pecan and white oak on an upland site. *Agroforestry Systems*, *88*(1), 141–155. https://doi.org/10.1007/s10457-013-9662-5

Chapin, F. S., Schulze, E. D., & Mooney, H. A. (1990). The ecology and economics of storage in plants. *Annual Review of Ecology and Systematics*, *21*, 423–447. https://doi.org/10.1146/annurev.ecolsys.21.1.423

Chen, D., Wang, S., Xiong, B., Cao, B., & Deng, X. (2015). Carbon/nitrogen imbalance associated with drought-induced leaf senescence in *Sorghum bicolor*. *PLoS ONE*, *10*(8), e0137026. https://doi.org/10.1371/journal.pone.0137026

Ciais, P., Sabine, C., Bala, G., Bopp, L., Brovkin, V., Canadell, J., … Heimann, M. (2014). Carbon and other biogeochemical cycles. In T. F. Stocker, D. Qin, G.-K. Plattner, M. Tignor, S. K. Allen, J. Boschung, … P. M. Midgley (Eds.), *Climate change 2013: The physical science basis. Contribution of working group I to the fifth assessment report of the Intergovernmental Panel on Climate Change* (pp. 465–570). Cambridge, UK: Cambridge University Press.

Cleland, E. E., Chuine, I., Menzel, A., Mooney, H. A., & Schwartz, M. D. (2007). Shifting plant phenology in response to global change. *Trends in Ecology & Evolution*, *22*(7), 357–365. https://doi.org/10.1016/j.tree.2007.04.003

Condit, R., Watts, K., Bohlman, S. A., Pérez, R., Foster, R. B., & Hubbell, S. P. (2000). Quantifying the deciduousness of tropical forest canopies under varying climates. *Journal of Vegetation Science*, *11*(5), 649–658. https://doi.org/10.2307/3236572

Croft, H., Chen, J. M., Froelich, N. J., Chen, B., & Staebler, R. M. (2015). Seasonal controls of canopy chlorophyll content on forest carbon uptake: Implications for GPP modeling. *Journal of Geophysical Research: Biogeosciences*, *120*(8), 1576–1586. https://doi.org/10.1002/2015jg002980

de Jong, R., Verbesselt, J., Schaepman, M. E., & de Bruin, S. (2012). Trend changes in global greening and browning: Contribution of short-term trends to longer-term change. *Global Change Biology*, *18*(2), 642–655. https://doi.org/10.1111/j.1365-2486.2011.02578.x

Diffenbaugh, N. S., Swain, D. L., & Touma, D. (2015). Anthropogenic warming has increased drought risk in California. *Proceedings of the National Academy of Sciences of the United States of America*, *112*(13), 3931–3936. https://doi.org/10.1073/pnas.1422385112

El-Madany, T. S., Reichstein, M., Perez-Priego, O., Carrara, A., Moreno, G., Pilar Martín, M., … Migliavacca, M. (2018). Drivers of spatio-temporal variability of carbon dioxide and energy fluxes in a Mediterranean savanna ecosystem. *Agricultural and Forest Meteorology*, *262*, 258–278. https://doi.org/10.1016/j.agrformet.2018.07.010

Fay, P. A., Prober, S. M., Harpole, W. S., Knops, J. M. H., Bakker, J. D., Borer, E. T., … Yang, L. H. (2015). Grassland productivity limited by multiple nutrients. *Nature Plants*, *1*(7), 15080. https://doi.org/10.1038/nplants.2015.80

Fensholt, R., Sandholt, I., & Rasmussen, M. S. (2004). Evaluation of MODIS LAI, fAPAR and the relation between fAPAR and NDVI in a semi-arid environment using in situ measurements. *Remote Sensing of Environment*, *91*(3–4), 490–507. https://doi.org/10.1016/j.rse.2004.04.009

Filippa, G., Cremonese, E., Migliavacca, M., Galvagno, M., Forkel, M., Wingate, L., … Richardson, A. D. (2016). Phenopix: AR

package for image-based vegetation phenology. *Agricultural and Forest Meteorology*, *220*, 141–150. https://doi.org/10.1016/j.agrformet.2016.01.006

Fleischer, K., Rebel, K. T., van der Molen, M. K., Erisman, J. W., Wassen, M. J., van Loon, E. E., … Dolman, A. J. (2013). The contribution of nitrogen deposition to the photosynthetic capacity of forests. *Global Biogeochemical Cycles*, *27*(1), 187–199. https://doi.org/10.1002/gbc.20026

Forkel, M., Migliavacca, M., Thonicke, K., Reichstein, M., Schaphoff, S., Weber, U., & Carvalhais, N. (2015). Codominant water control on global interannual variability and trends in land surface phenology and greenness. *Global Change Biology*, *21*(9), 3414–3435. https://doi.org/10.1111/gcb.12950

Fu, Z., Stoy, P. C., Poulter, B., Gerken, T., Zhang, Z., Wakbulcho, G., & Niu, S. (2019). Maximum carbon uptake rate dominates the interannual variability of global net ecosystem exchange. *Global Change Biology*, *25*(10), 3381–3394. https://doi.org/10.1111/gcb.14731

García, M., Gajardo, J., Riaño, D., Zhao, K., Martín, P., & Ustin, S. (2015). Canopy clumping appraisal using terrestrial and airborne laser scanning. *Remote Sensing of Environment*, *161*, 78–88. https://doi.org/10.1016/j.rse.2015.01.030

Gerard, F. F., George, C. T., Hayman, G., Chavana-Bryant, C., & Weedon, G. P. (2020). Leaf phenology amplitude derived from MODIS NDVI and EVI: Maps of leaf phenology synchrony for Meso- and South America. *Geoscience Data Journal*. https://doi.org/10.1002/gdj3.87

Gitelson, A. A., Viña, A., Ciganda, V., Rundquist, D. C., & Arkebauer, T. J. (2005). Remote estimation of canopy chlorophyll content in crops. *Geophysical Research Letters*, *32*(8). https://doi.org/10.1029/2005gl022688

Gong, X. Y., Fanselow, N., Dittert, K., Taube, F., & Lin, S. (2015). Response of primary production and biomass allocation to nitrogen and water supplementation along a grazing intensity gradient in semiarid grassland. *European Journal of Agronomy*, *63*, 27–35. https://doi.org/10.1016/j.eja.2014.11.004

Grossiord, C., Sevanto, S., Adams, H. D., Collins, A. D., Dickman, L. T., McBranch, N., … McDowell, N. G. (2017). Precipitation, not air temperature, drives functional responses of trees in semi-arid ecosystems. *Journal of Ecology*, *105*(1), 163–175. https://doi.org/10.1111/1365-2745.12662

Guo, Q., Hu, Z.-M., Li, S.-G., Yu, G.-R., Sun, X.-M., Li, L.-H., … Bai, W.-M. (2016). Exogenous N addition enhances the responses of gross primary productivity to individual precipitation events in a temperate grassland. *Scientific Reports*, *6*, 26901. https://doi.org/10.1038/srep26901

Guo, Q., Li, S., Hu, Z., Zhao, W., Yu, G., Sun, X., … Bai, W. (2016). Responses of gross primary productivity to different sizes of precipitation events in a temperate grassland ecosystem in Inner Mongolia, China. *Journal of Arid Land*, *8*(1), 36–46. https://doi.org/10.1007/s40333-015-0136-7

Harper, C. W., Blair, J. M., Fay, P. A., Knapp, A. K., & Carlisle, J. D. (2005). Increased rainfall variability and reduced rainfall amount decreases soil CO_2 flux in a grassland ecosystem. *Global Change Biology*, *11*(2), 322–334. https://doi.org/10.1111/j.1365-2486.2005.00899.x

Harpole, W. S., Potts, D. L., & Suding, K. N. (2007). Ecosystem responses to water and nitrogen amendment in a California grassland. *Global Change Biology*, *13*(11), 2341–2348. https://doi.org/10.1111/j.1365-2486.2007.01447.x

Hernández, I., Alegre, L., & Munné-Bosch, S. (2004). Drought-induced changes in flavonoids and other low molecular weight antioxidants in *Cistus clusii* grown under Mediterranean field conditions. *Tree Physiology*, *24*(11), 1303–1311. https://doi.org/10.1093/treephys/24.11.1303

Hsiao, T. C. (1973). Plant responses to water stress. *Annual Review of Plant Physiology*, *24*(1), 519–570. https://doi.org/10.1146/annurev.pp.24.060173.002511

Hu, B., & Chu, C. (2019). Nitrogen–phosphorus interplay: Old story with molecular tale. *New Phytologist*. https://doi.org/10.1111/nph.16102

Hu, Z., Shi, H., Cheng, K., Wang, Y.-P., Piao, S., Li, Y., … Yu, G. (2018). Joint structural and physiological control on the interannual variation in productivity in a temperate grassland: A data-model comparison. *Global Change Biology*, *24*(7), 2965–2979. https://doi.org/10.1111/gcb.14274

Huxman, T. E., Snyder, K. A., Tissue, D., Leffler, A. J., Ogle, K., Pockman, W. T., … Schwinning, S. (2004). Precipitation pulses and carbon fluxes in semiarid and arid ecosystems. *Oecologia*, *141*(2), 254–268. https://doi.org/10.1007/s00442-004-1682-4

Intergovernmental Panel on Climate Change. (2013). *The physical science basis. Contribution of working group I to the fifth assessment report of the Intergovernmental Panel on Climate Change* (T. F. Stocker, D. Qin, G.-K. Plattner, M. Tignor, S. K. Allen, J. Boschung, … P. M. Midgley, Eds.) (pp. 33–118). Cambridge, UK: Cambridge University Press.

Isbell, F., Reich, P. B., Tilman, D., Hobbie, S. E., Polasky, S., & Binder, S. (2013). Nutrient enrichment, biodiversity loss, and consequent declines in ecosystem productivity. *Proceedings of the National Academy of Sciences of the United States of America*, *110*(29), 11911–11916. https://doi.org/10.1073/pnas.1310880110

Janssens, I. A., Dieleman, W., Luyssaert, S., Subke, J.-A., Reichstein, M., Ceulemans, R., … Law, B. E. (2010). Reduction of forest soil respiration in response to nitrogen deposition. *Nature Geoscience*, *3*(5), 315–322. https://doi.org/10.1038/ngeo844

Jing, H., Zhou, H., Wang, G., Xue, S., Liu, G., & Duan, M. (2017). Nitrogen addition changes the stoichiometry and growth rate of different organs in *Pinus tabuliformis* seedlings. *Frontiers in Plant Science*, *8*, 1922–1922. https://doi.org/10.3389/fpls.2017.01922

Jolly, W. M., & Running, S. W. (2004). Effects of precipitation and soil water potential on drought deciduous phenology in the Kalahari. *Global Change Biology*, *10*(3), 303–308. https://doi.org/10.1046/j.1365-2486.2003.00701.x

Jung, M., Reichstein, M., Schwalm, C. R., Huntingford, C., Sitch, S., Ahlström, A., … Zeng, N. (2017). Compensatory water effects link yearly global land CO_2 sink changes to temperature. *Nature*, *541*(7638), 516–520. https://doi.org/10.1038/nature20780

Kurc, S. A., & Benton, L. M. (2010). Digital image-derived greenness links deep soil moisture to carbon uptake in a creosotebush-dominated shrubland. *Journal of Arid Environments*, *74*(5), 585–594. https://doi.org/10.1016/j.jaridenv.2009.10.003

LeBauer, D. S., & Treseder, K. K. (2008). Nitrogen limitation of net primary productivity in terrestrial ecosystems is globally distributed. *Ecology*, *89*(2), 371–379. https://doi.org/10.1890/06-2057.1

Lee, M., Manning, P., Rist, J., Power, S. A., & Marsh, C. (2010). A global comparison of grassland biomass responses to CO_2 and nitrogen enrichment. *Philosophical Transactions of the Royal Society of London. Series B: Biological Sciences*, *365*(1549), 2047–2056. https://doi.org/10.1098/rstb.2010.0028

Liu, Q., Fu, Y. H., Zhu, Z., Liu, Y., Liu, Z., Huang, M., … Piao, S. (2016). Delayed autumn phenology in the Northern Hemisphere is related to change in both climate and spring phenology. *Global Change Biology*, *22*(11), 3702–3711. https://doi.org/10.1111/gcb.13311

Loladze, I., & Elser, J. J. (2011). The origins of the Redfield nitrogen-to-phosphorus ratio are in a homoeostatic protein-to-rRNA ratio. *Ecology Letters*, *14*(3), 244–250. https://doi.org/10.1111/j.1461-0248.2010.01577.x

Luo, Y., El-Madany, T. S., Filippa, G., Ma, X., Ahrens, B., Carrara, A., … Migliavacca, M. (2018). Using near-infrared-enabled digital repeat photography to track structural and physiological phenology in Mediterranean tree-grass ecosystems. *Remote Sensing*, *10*(8), 1293. https://doi.org/10.3390/rs10081293

Ma, X. L., Huete, A., Moran, S., Ponce-Campos, G., & Eamus, D. (2015). Abrupt shifts in phenology and vegetation productivity under

climate extremes. *Journal of Geophysical Research: Biogeosciences*, *120*(10), 2036–2052. https://doi.org/10.1002/2015jg003144

Mahowald, N., Jickells, T. D., Baker, A. R., Artaxo, P., Benitez-Nelson, C. R., Bergametti, G., … Tsukuda, S. (2008). Global distribution of atmospheric phosphorus sources, concentrations and deposition rates, and anthropogenic impacts. *Global Biogeochemical Cycles*, *22*(4). https://doi.org/10.1029/2008gb003240

Marcolla, B., Cescatti, A., Manca, G., Zorer, R., Cavagna, M., Fiora, A., … Zampedri, R. (2011). Climatic controls and ecosystem responses drive the inter-annual variability of the net ecosystem exchange of an alpine meadow. *Agricultural and Forest Meteorology*, *151*(9), 1233–1243. https://doi.org/10.1016/j.agrformet.2011.04.015

Martini, D., Pacheco-Labrador, J., Perez-Priego, O., van der Tol, C., El-Madany, T. S., Julitta, T., … Moreno, G. (2019). Nitrogen and phosphorus effect on sun-induced fluorescence and gross primary productivity in Mediterranean grassland. *Remote Sensing*, *11*(21), 2562. https://doi.org/10.3390/rs11212562

Matzek, V., & Vitousek, P. M. (2009). N:P stoichiometry and protein: RNA ratios in vascular plants: An evaluation of the growth-rate hypothesis. *Ecology Letters*, *12*(8), 765–771. https://doi.org/10.1111/j.1461-0248.2009.01310.x

Mauder, M., & Foken, T. (2011). *Documentation and instruction manual of the eddy-covariance software package TK3*. Retrieved from http://nbn-resolving.org/urn:nbn:de:bvb:703-opus-8665

Mazdiyasni, O., & AghaKouchak, A. (2015). Substantial increase in concurrent droughts and heatwaves in the United States. *Proceedings of the National Academy of Sciences of the United States of America*, *112*(37), 11484–11489. https://doi.org/10.1073/pnas.1422945112

Melendo-Vega, J., Martín, M., Pacheco-Labrador, J., González-Cascón, R., Moreno, G., Pérez, F., … Riaño, D. (2018). Improving the performance of 3-D radiative transfer model FLIGHT to simulate optical properties of a tree-grass ecosystem. *Remote Sensing*, *10*(12), 2061. https://doi.org/10.3390/rs10122061

Menzel, A., Sparks, T. H., Estrella, N., Koch, E., Aasa, A., Ahas, R., … Zust, A. (2006). European phenological response to climate change matches the warming pattern. *Global Change Biology*, *12*(10), 1969–1976. https://doi.org/10.1111/j.1365-2486.2006.01193.x

Meza, F. J., Montes, C., Bravo-Martínez, F., Serrano-Ortiz, P., & Kowalski, A. S. (2018). Soil water content effects on net ecosystem CO_2 exchange and actual evapotranspiration in a Mediterranean semiarid savanna of Central Chile. *Scientific Reports*, *8*(1), 8570. https://doi.org/10.1038/s41598-018-26934-z

Migliavacca, M., Galvagno, M., Cremonese, E., Rossini, M., Meroni, M., Sonnentag, O., … Richardson, A. D. (2011). Using digital repeat photography and eddy covariance data to model grassland phenology and photosynthetic CO_2 uptake. *Agricultural and Forest Meteorology*, *151*(10), 1325–1337. https://doi.org/10.1016/j.agrformet.2011.05.012

Migliavacca, M., Perez-Priego, O., Rossini, M., El-Madany, T. S., Moreno, G., van der Tol, C., … Reichstein, M. (2017). Plant functional traits and canopy structure control the relationship between photosynthetic CO_2 uptake and far-red sun-induced fluorescence in a Mediterranean grassland under different nutrient availability. *New Phytologist*, *214*(3), 1078–1091. https://doi.org/10.1111/nph.14437

Migliavacca, M., Reichstein, M., Richardson, A. D., Mahecha, M. D., Cremonese, E., Delpierre, N., … Cescatti, A. (2015). Influence of physiological phenology on the seasonal pattern of ecosystem respiration in deciduous forests. *Global Change Biology*, *21*(1), 363–376. https://doi.org/10.1111/gcb.12671

Montaldo, N., Albertson, J. D., & Mancini, M. (2008). Vegetation dynamics and soil water balance in a water-limited Mediterranean ecosystem on Sardinia, Italy. *Hydrology and Earth System Sciences Discussions*, *5*(1), 219–255. https://doi.org/10.5194/hessd-5-219-2008

Monteith, J. (1972). Solar radiation and productivity in tropical ecosystems. *Journal of Applied Ecology*, *9*(3), 747–766. https://doi.org/10.2307/2401901

Moreno, G. (2008). Response of understorey forage to multiple tree effects in Iberian dehesas. *Agriculture, Ecosystems & Environment*, *123*(1), 239–244. https://doi.org/10.1016/j.agee.2007.04.006

Morris, K. A., Nair, R. K. F., Moreno, G., Schrumpf, M., & Migliavacca, M. (2019). Fate of N additions in a multiple resource-limited Mediterranean oak savanna. *Ecosphere*, *10*(11), e02921. https://doi.org/10.1002/ecs2.2921

Nair, R. K. F., Morris, K. A., Hertel, M., Luo, Y., Moreno, G., Reichstein, M., … Migliavacca, M. (2019). N: P stoichiometry and habitat effects on Mediterranean savanna seasonal root dynamics. *Biogeosciences*, *16*(9), 1883–1901. https://doi.org/10.5194/bg-16-1883-2019

Nelson, J. A., Carvalhais, N., Cuntz, M., Delpierre, N., Knauer, J., Ogée, J., … Jung, M. (2018). Coupling water and carbon fluxes to constrain estimates of transpiration: The TEA algorithm. *Journal of Geophysical Research: Biogeosciences*, *123*(12), 3617–3632. https://doi.org/10.1029/2018jg004727

Niu, S., Yang, H., Zhang, Z., Wu, M., Lu, Q. I., Li, L., … Wan, S. (2009). Non-additive effects of water and nitrogen addition on ecosystem carbon exchange in a temperate steppe. *Ecosystems*, *12*(6), 915–926. https://doi.org/10.1007/s10021-009-9265-1

Nomura, N., & Kikuzawa, K. (2003). Productive phenology of tropical montane forests: Fertilization experiments along a moisture gradient. *Ecological Research*, *18*(5), 573–586. https://doi.org/10.1046/j.1440-1703.2003.00579.x

Pacheco-Labrador, J.,Perez-Priego, O.,El-Madany, T. S., Julitta, T., Rossini, M., Guan, J., … Migliavacca, M. (2019). Multiple-constraint inversion of SCOPE. Evaluating the potential of GPP and SIF for the retrieval of plant functional traits. *Remote Sensing of Environment*, *234*. https://doi.org/10.1016/j.rse.2019.111362

Papale, D., Reichstein, M., Aubinet, M., Canfora, E., Bernhofer, C., Kutsch, W., … Yakir, D. (2006). Towards a standardized processing of Net Ecosystem Exchange measured with eddy covariance technique: Algorithms and uncertainty estimation. *Biogeosciences*, *3*(4), 571–583. https://doi.org/10.5194/bg-3-571-2006

Peñuelas, J., Poulter, B., Sardans, J., Ciais, P., van der Velde, M., Bopp, L., … Janssens, I. A. (2013). Human-induced nitrogen–phosphorus imbalances alter natural and managed ecosystems across the globe. *Nature Communications*, *4*(1), 2934. https://doi.org/10.1038/ncomms3934

Peñuelas, J., Sardans, J., Rivas-ubach, A., & Janssens, I. A. (2012). The human-induced imbalance between C, N and P in Earth's life system. *Global Change Biology*, *18*(1), 3–6. https://doi.org/10.1111/j.1365-2486.2011.02568.x

Perez-Priego, O., El-Madany, T. S., Migliavacca, M., Kowalski, A. S., Jung, M., Carrara, A., … Reichstein, M. (2017). Evaluation of eddy covariance latent heat fluxes with independent lysimeter and sapflow estimates in a Mediterranean savannah ecosystem. *Agricultural and Forest Meteorology*, *236*, 87–99. https://doi.org/10.1016/j.agrformet.2017.01.009

Perez-Priego, O., Guan, J., Rossini, M., Fava, F., Wutzler, T., Moreno, G., … Migliavacca, M. (2015). Sun-induced chlorophyll fluorescence and photochemical reflectance index improve remote-sensing gross primary production estimates under varying nutrient availability in a typical Mediterranean savanna ecosystem. *Biogeosciences*, *12*(21), 6351–6367. https://doi.org/10.5194/bg-12-6351-2015

Piao, S., Liu, Q., Chen, A., Janssens, I. A., Fu, Y., Dai, J., … Zhu, X. (2019). Plant phenology and global climate change: Current progresses and challenges. *Global Change Biology*, *25*(6), 1922–1940. https://doi.org/10.1111/gcb.14619

Pic, E., de La Serve, B. T., Tardieu, F., & Turc, O. (2002). Leaf senescence induced by mild water deficit follows the same sequence of macroscopic, biochemical, and molecular events as monocarpic senescence

in pea. *Plant Physiology*, *128*(1), 236–246. https://doi.org/10.1104/pp.010634

Poulter, B., Frank, D., Ciais, P., Myneni, R. B., Andela, N., Bi, J., … van der Werf, G. R. (2014). Contribution of semi-arid ecosystems to interannual variability of the global carbon cycle. *Nature*, *509*, 600–603. https://doi.org/10.1038/nature13376

Reay, D. S., Dentener, F., Smith, P., Grace, J., & Feely, R. A. (2008). Global nitrogen deposition and carbon sinks. *Nature Geoscience*, *1*(7), 430–437. https://doi.org/10.1038/ngeo230

Rebmann, C., Göckede, M., Foken, T., Aubinet, M., Aurela, M., Berbigier, P., … Yakir, D. (2005). Quality analysis applied on eddy covariance measurements at complex forest sites using footprint modelling. *Theoretical and Applied Climatology*, *80*(2–4), 121–141. https://doi.org/10.1007/s00704-004-0095-y

Reichstein, M., Bahn, M., Mahecha, M. D., Kattge, J., & Baldocchi, D. D. (2014). Linking plant and ecosystem functional biogeography. *Proceedings of the National Academy of Sciences of the United States of America*, *111*(38), 13697–13702. https://doi.org/10.1073/pnas.1216065111

Reichstein, M., Falge, E., Baldocchi, D., Papale, D., Aubinet, M., Berbigier, P., … Valentini, R. (2005). On the separation of net ecosystem exchange into assimilation and ecosystem respiration: Review and improved algorithm. *Global Change Biology*, *11*(9), 1424–1439. https://doi.org/10.1111/j.1365-2486.2005.001002.x

Reynolds, J. F., Kemp, P. R., Ogle, K., & Fernández, R. J. (2004). Modifying the 'pulse–reserve' paradigm for deserts of North America: Precipitation pulses, soil water, and plant responses. *Oecologia*, *141*(2), 194–210. https://doi.org/10.1007/s00442-004-1524-4

Richardson, A. D. (2019). Tracking seasonal rhythms of plants in diverse ecosystems with digital camera imagery. *New Phytologist*, *222*(4), 1742–1750. https://doi.org/10.1111/nph.15591

Richardson, A. D., Andy Black, T., Ciais, P., Delbart, N., Friedl, M. A., Gobron, N., … Varlagin, A. (2010). Influence of spring and autumn phenological transitions on forest ecosystem productivity. *Philosophical Transactions of the Royal Society B: Biological Sciences*, *365*(1555), 3227–3246. https://doi.org/10.1098/rstb.2010.0102

Richardson, A. D., Braswell, B. H., Hollinger, D. Y., Jenkins, J. P., & Ollinger, S. V. (2009). Near-surface remote sensing of spatial and temporal variation in canopy phenology. *Ecological Applications*, *19*(6), 1417–1428. https://doi.org/10.1890/08-2022.1

Richardson, A. D., Hollinger, D. Y., Aber, J. D., Ollinger, S. V., & Braswell, B. H. (2007). Environmental variation is directly responsible for short- but not long-term variation in forest-atmosphere carbon exchange. *Global Change Biology*, *13*(4), 788–803. https://doi.org/10.1111/j.1365-2486.2007.01330.x

Richardson, A. D., Hufkens, K., Milliman, T., Aubrecht, D. M., Chen, M., Gray, J. M., … Frolking, S. (2018). Tracking vegetation phenology across diverse North American biomes using PhenoCam imagery. *Scientific Data*, *5*, 180028. https://doi.org/10.1038/sdata.2018.28

Richardson, A. D., Keenan, T. F., Migliavacca, M., Ryu, Y., Sonnentag, O., & Toomey, M. (2013). Climate change, phenology, and phenological control of vegetation feedbacks to the climate system. *Agricultural and Forest Meteorology*, *169*, 156–173. https://doi.org/10.1016/j.agrformet.2012.09.012

Rishmawi, K., Prince, S. D., & Xue, Y. (2016). Vegetation responses to climate variability in the northern arid to sub-humid zones of Sub-Saharan Africa. *Remote Sensing*, *8*(11), 910. https://doi.org/10.3390/rs8110910

Rivas-Ubach, A., Sardans, J., Pérez-Trujillo, M., Estiarte, M., & Peñuelas, J. (2012). Strong relationship between elemental stoichiometry and metabolome in plants. *Proceedings of the National Academy of Sciences of the United States of America*, *109*(11), 4181–4186. https://doi.org/10.1073/pnas.1116092109

Sardans, J., & Peñuelas, J. (2013). Plant-soil interactions in Mediterranean forest and shrublands: Impacts of climatic change. *Plant and Soil*, *365*(1), 1–33. https://doi.org/10.1007/s11104-013-1591-6

Schlemmer, M. R., Francis, D. D., Shanahan, J. F., & Schepers, J. S. (2005). Remotely measuring chlorophyll content in corn leaves with differing nitrogen levels and relative water content. *Agronomy Journal*, *97*(1), 106–112. https://doi.org/10.2134/agronj2005.0106

Serrano, L., Filella, I., & Peñuelas, J. (2000). Remote sensing of biomass and yield of winter wheat under different nitrogen supplies. *Crop Science*, *40*(3), 723–731. https://doi.org/10.2135/cropsci2000.403723x

Sonnentag, O., Hufkens, K., Teshera-Sterne, C., Young, A. M., Friedl, M., Braswell, B. H., … Richardson, A. D. (2012). Digital repeat photography for phenological research in forest ecosystems. *Agricultural and Forest Meteorology*, *152*, 159–177. https://doi.org/10.1016/j.agrformet.2011.09.009

Soons, M. B., Hefting, M. M., Dorland, E., Lamers, L. P. M., Versteeg, C., & Bobbink, R. (2017). Nitrogen effects on plant species richness in herbaceous communities are more widespread and stronger than those of phosphorus. *Biological Conservation*, *212*, 390–397. https://doi.org/10.1016/j.biocon.2016.12.006

Soudani, K., Hmimina, G., Delpierre, N., Pontailler, J.-Y., Aubinet, M., Bonal, D., … Dufrêne, E. (2012). Ground-based Network of NDVI measurements for tracking temporal dynamics of canopy structure and vegetation phenology in different biomes. *Remote Sensing of Environment*, *123*, 234–245. https://doi.org/10.1016/j.rse.2012.03.012

Svoray, T., & Karnieli, A. (2011). Rainfall, topography and primary production relationships in a semiarid ecosystem. *Ecohydrology*, *4*(1), 56–66. https://doi.org/10.1002/eco.123

Tatarko, A. R. (2017). Master thesis: Nitrogen addition and ecosystem functioning: Changes in species composition leaf traits amplify increases in leaf area index and canopy chlorophyll.

Tilman, D. (1987). Secondary succession and the pattern of plant dominance along experimental nitrogen gradients. *Ecological Monographs*, *57*(3), 189–214. https://doi.org/10.2307/2937080

Tramontana, G., Jung, M., Schwalm, C. R., Ichii, K., Camps-Valls, G., Ráduly, B., … Papale, D. (2016). Predicting carbon dioxide and energy fluxes across global FLUXNET sites with regression algorithms. *Biogeosciences*, *13*(14), 4291–4313. https://doi.org/10.5194/bg-13-4291-2016

Tucker, C. J. (1979). Red and photographic infrared linear combinations for monitoring vegetation. *Remote Sensing of Environment*, *8*(2), 127–150. https://doi.org/10.1016/0034-4257(79)90013-0

Wang, C., & Tang, Y. (2019). Responses of plant phenology to nitrogen addition: A meta-analysis. *Oikos*, *128*(9), 1243–1253. https://doi.org/10.1111/oik.06099

Wang, M., Shi, S., Lin, F., Hao, Z. Q., Jiang, P., & Dai, G. H. (2012). Effects of soil water and nitrogen on growth and photosynthetic response of Manchurian Ash (*Fraxinus mandshurica*) seedlings in Northeastern China. *PLoS ONE*, *7*(2). https://doi.org/10.1371/journal.pone.0030754

Wang, X. H., Piao, S. L., Xu, X. T., Ciais, P., MacBean, N., Myneni, R. B., & Li, L. (2015). Has the advancing onset of spring vegetation green-up slowed down or changed abruptly over the last three decades? *Global Ecology and Biogeography*, *24*(6), 621–631. https://doi.org/10.1111/geb.12289

Wingate, L., Ogée, J., Cremonese, E., Filippa, G., Mizunuma, T., Migliavacca, M., … Grace, J. (2015). Interpreting canopy development and physiology using a European phenology camera network at flux sites. *Biogeosciences*, *12*(20), 5995–6015. https://doi.org/10.5194/bg-12-5995-2015

Wu, J., van der Linden, L., Lasslop, G., Carvalhais, N., Pilegaard, K., Beier, C., & Ibrom, A. (2012). Effects of climate variability and functional changes on the interannual variation of the carbon balance in a temperate deciduous forest. *Biogeosciences*, *9*(1), 13–28. https://doi.org/10.5194/bg-9-13-2012

Wutzler, T., Lucas-Moffat, A., Migliavacca, M., Knauer, J., Sickel, K., Šigut, L., … Reichstein, M. (2018). Basic and extensible post-processing of

eddy covariance flux data with REddyProc. *Biogeosciences*, *15*(16), 5015–5030. https://doi.org/10.5194/bg-15-5015-2018

Xia, J., Niu, S., Ciais, P., Janssens, I. A., Chen, J., Ammann, C., … Luo, Y. (2015). Joint control of terrestrial gross primary productivity by plant phenology and physiology. *Proceedings of the National Academy of Sciences of the United States of America*, *112*(9), 2788–2793. https://doi.org/10.1073/pnas.1413090112

Xia, J., & Wan, S. (2013). Independent effects of warming and nitrogen addition on plant phenology in the Inner Mongolian steppe. *Annals of Botany*, *111*(6), 1207–1217. https://doi.org/10.1093/aob/mct079

Xu, L., & Baldocchi, D. D. (2004). Seasonal variation in carbon dioxide exchange over a Mediterranean annual grassland in California. *Agricultural and Forest Meteorology*, *123*(1), 79–96. https://doi.org/10.1016/j.agrformet.2003.10.004

Xu, X., Medvigy, D., Powers, J. S., Becknell, J. M., & Guan, K. (2016). Diversity in plant hydraulic traits explains seasonal and inter-annual variations of vegetation dynamics in seasonally dry tropical forests. *New Phytologist*, *212*(1), 80–95. https://doi.org/10.1111/nph.14009

Yang, N., Zavišić, A., Pena, R., & Polle, A. (2016). Phenology, photosynthesis, and phosphorus in European beech (*Fagus sylvatica* L.) in two forest soils with contrasting P contents. *Journal of Plant Nutrition and Soil Science*, *179*(2), 151–158. https://doi.org/10.1002/jpln.201500539

Yang, X., Tang, J., & Mustard, J. F. (2014). Beyond leaf color: Comparing camera-based phenological metrics with leaf biochemical, biophysical, and spectral properties throughout the growing season of a temperate deciduous forest. *Journal of Geophysical Research: Biogeosciences*, *119*(3), 181–191. https://doi.org/10.1002/2013jg002460

Yin, T.-F., Zheng, L.-L., Cao, G.-M., Song, M.-H., & Yu, F.-H. (2016). Species-specific phenological responses to long-term nitrogen fertilization in an alpine meadow. *Journal of Plant Ecology*, *10*(2), 301–309. https://doi.org/10.1093/jpe/rtw026

Zeileis, A., & Grothendieck, G. (2005). zoo: S3 infrastructure for regular and irregular time series. *Journal of Statistical Software*, *14*(6), 1–27.

Zeng, N., Mariotti, A., & Wetzel, P. (2005). Terrestrial mechanisms of interannual CO_2 variability. *Global Biogeochemical Cycles*, *19*(1). https://doi.org/10.1029/2004gb002273

Zhang, R., & Wienhold, B. J. (2002). The effect of soil moisture on mineral nitrogen, soil electrical conductivity, and pH. *Nutrient Cycling in Agroecosystems*, *63*(2–3), 251–254. https://doi.org/10.1023/a:1021115227884

Zhang, X., Friedl, M. A., Schaaf, C. B., Strahler, A. H., Hodges, J. C. F., Gao, F., … Huete, A. (2003). Monitoring vegetation phenology using MODIS. *Remote Sensing of Environment*, *84*(3), 471–475. https://doi.org/10.1016/s0034-4257(02)00135-9

Zhou, S., Zhang, Y., Park Williams, A., & Gentine, P. (2019). Projected increases in intensity, frequency, and terrestrial carbon costs of compound drought and aridity events. *Science Advances*, *5*(1), eaau5740. https://doi.org/10.1126/sciadv.aau5740

SUPPORTING INFORMATION

Additional supporting information may be found online in the Supporting Information section.

How to cite this article: Luo Y, El-Madany T, Ma X, et al. Nutrients and water availability constrain the seasonality of vegetation activity in a Mediterranean ecosystem. *Glob Change Biol.* 2020;26:4379–4400. https://doi.org/10.1111/gcb.15138